



HAL
open science

Modality-independent effect of gravity in shaping the internal representation of 3D space for visual and haptic object perception

Theo Morfoisse, Gabriela Herrera Altamira, Leonardo Angelini, Gilles Clément, Mathieu Beraneck, Joseph McIntyre, Michele Tagliabue

► To cite this version:

Theo Morfoisse, Gabriela Herrera Altamira, Leonardo Angelini, Gilles Clément, Mathieu Beraneck, et al.. Modality-independent effect of gravity in shaping the internal representation of 3D space for visual and haptic object perception. *Journal of Neuroscience*, 2024, pp.e2457202023. 10.1523/JNEUROSCI.2457-20.2023 . hal-04515112

HAL Id: hal-04515112

<https://hal.science/hal-04515112v1>

Submitted on 21 Mar 2024

HAL is a multi-disciplinary open access archive for the deposit and dissemination of scientific research documents, whether they are published or not. The documents may come from teaching and research institutions in France or abroad, or from public or private research centers.

L'archive ouverte pluridisciplinaire **HAL**, est destinée au dépôt et à la diffusion de documents scientifiques de niveau recherche, publiés ou non, émanant des établissements d'enseignement et de recherche français ou étrangers, des laboratoires publics ou privés.

Research Articles | Behavioral/Cognitive

Modality-independent effect of gravity in shaping the internal representation of 3D space for visual and haptic object perception

<https://doi.org/10.1523/JNEUROSCI.2457-20.2023>

Received: 12 August 2020

Revised: 20 December 2023

Accepted: 22 December 2023

Copyright © 2024 the authors

This Early Release article has been peer reviewed and accepted, but has not been through the composition and copyediting processes. The final version may differ slightly in style or formatting and will contain links to any extended data.

Alerts: Sign up at www.jneurosci.org/alerts to receive customized email alerts when the fully formatted version of this article is published.

1 **Modality-independent effect of gravity in shaping the**
2 **internal representation of 3D space for visual and haptic**
3 **object perception**

4
5 Abbreviated title:

6 **Gravity's effect on internal representation of space**

7
8 Theo Morfousse^{1,#}, Gabriela Herrera Altamira^{1,#}, Leonardo Angelini^{2,3}, Gilles Clément⁴, Mathieu Beraneck¹, Joseph
9 McIntyre^{1,5}, Michele Tagliabue^{1*}

10 # These authors contributed equally

- 11 1 Université Paris Cité, CNRS UMR 8002, INCC - Integrative Neuroscience and Cognition Center, F-75006,
12 Paris, France.
13 2 HumanTech Institute, University of Applied Sciences Western Switzerland//HES-SO, 1700 Fribourg,
14 Switzerland
15 3 School of Management Fribourg, University of Applied Sciences Western Switzerland//HES-SO, 1700
16 Fribourg, Switzerland
17 4 Université de Caen Normandie, Inserm, COMETE U1075, CYCERON, CHU de Caen, Normandie Univ,
18 14000, Caen, France.
19 5 Tecnalia, Basque Research and Technology Alliance, 20009, San Sebastian, Spain

20
21
22 * **Corresponding author:** Michele Tagliabue; 45 rue des St-Pères; Université Paris Cité, Integrative Neuroscience and
23 Cognition Center, CNRS UMR 8002, F-75270 Paris, France. E-mail: michele.tagliabue@parisdescartes.fr

24 Number of figures: 9

25 Number of tables: 3

26 Number of words for Abstract : 206

27 Introduction : 593

28 Discussion : 1500

29 **Acknowledgment:** The authors thank M. Mark Wexler and M Patrice Senot for useful discussions about data analyses
30 and M. Patrice Jegouzo for his technical help in designing the experimental setup. We also acknowledge the 'Plateforme

31 PES' core facility of BioMedTech Facilities INSERM US36 | CNRS UAR2009 | Université Paris Cité for contributing to the
32 experimental setup. This work was supported by the Centre National des Etudes Spatiales. This study contributes to the
33 IdEx Université de Paris ANR-18-IDEX-0001.

JNeurosci Accepted Manuscript

34 **Abstract**

35 Visual and haptic perceptions of 3D shape are plagued by distortions, which are influenced by
36 non-visual factors, such as gravitational vestibular signals. Whether gravity acts directly on the
37 visual or haptic systems or at a higher, modality-independent level of information processing
38 remains unknown. To test these hypotheses, we examined visual and haptic 3D shape perception
39 by asking male and female human subjects to perform a “squaring” task in upright and supine
40 postures and in microgravity. Subjects adjusted one edge of a 3D object to match the length of
41 another in each of the 3 canonical reference planes and we recorded the matching errors to obtain
42 a characterization of the perceived 3D shape. The results show opposing, body-centered patterns
43 of errors for visual and haptic modalities, whose amplitudes are negatively correlated, suggesting
44 that they arise in distinct modality-specific representations that are nevertheless linked at some
45 level. On the other hand, weightlessness significantly modulated both visual and haptic
46 perceptual distortions in the same way, indicating a common, modality-independent origin for
47 gravity’s effects. Overall, our findings show a link between modality-specific visual and haptic
48 perceptual distortions and demonstrate a role of gravity-related signals on a modality-
49 independent internal representation of the body and peripersonal 3D space used to interpret
50 incoming sensory inputs.

51 **Significance Statement**

52 Both visual and haptic 3D-object perception are plagued by anisotropic patterns of errors, as shown in a
53 task of “squaring” the faces of an adjustable cube.

54 We report opposing and negatively correlated perceptive errors for the visual and haptic perceptions,
55 suggesting a strong interaction between the two sensory modalities, even when the task was
56 fundamentally unimodal.

57 In addition, the similar effect of microgravity observed on both visual and haptic perception indicates that
58 gravity acts on a modality-independent representation of 3D space used to process these sensory inputs.

59 These findings foster awareness that even simple, unimodal, egocentric tasks are likely to involve complex,
60 cross-modal signal processing.

61 Introduction

62 Perception of three-dimensional (3D) objects includes the ability to determine an item's location
63 in space, as well as its geometrical properties, such as the relative size along each of three
64 dimensions and the relative orientation of its edges. Given its importance for interacting with the
65 physical world, 3D object perception has been deeply investigated. Visual perception has received
66 the most attention, showing how various features of the stimuli, such as disparities, size,
67 occlusions, perspective, motion, shadows, shading, texture and blur, all influence 3D visual
68 perception (Welchman, 2016) and how *internal models* shape the interpretation of the sensory
69 signals (Curry, 1972; Kersten and Yuille, 2003; Kersten et al., 2004; Lee, 2015).

70 Despite its critical importance to perception and action, visual perception suffers from measurable
71 distortions: i.e. height underestimation with respect to width, also known as the horizontal-
72 vertical, or "L", illusion (Avery and Day, 1969) and a systematic underestimation of depth (Loomis
73 and Philbeck, 1999; Todd and Norman, 2003). Non-visual factors, such as gravity, also appear to
74 affect visual perception. For example, tilting the body with respect to gravity affects object
75 recognition (Leone, 1998; Barnett-Cowan et al., 2015), orientation and distance perception
76 (Marendaz et al., 1993; Harris and Mander, 2014), and other phenomena such as the tilted frame
77 illusion (Goodenough et al., 1981; Howard, 1982), the oblique effect (Lipshits and McIntyre, 1999;
78 Luyat and Gentaz, 2002; McIntyre and Lipshits, 2008) and some geometric illusions (Prinzmetal
79 and Beck, 2001; Clément and Eckardt, 2005). Furthermore, weightlessness significantly alters the
80 perception of stimulus size and shape, especially in tasks involving depth, during both short-term
81 (Villard et al., 2005; Clément and Buckley, 2008; Clément et al., 2008; Harris et al., 2010; Clément
82 and Demel, 2012; Clément et al., 2016; Bourrelly et al., 2016) and long-term (Clément et al., 2012,
83 2013; De Saedeleer et al., 2013; Bourrelly et al., 2015) exposure.

84 One hypothesis to explain gravity-related changes in visual perception is that gravity affects both
85 the eye movements underlying visual exploration (Clément et al., 1986; Reschke et al., 2017,
86 2018) and eye positioning that contributes to the estimation of the visual eye-height, a key
87 reference within the visual scene (Goltz et al., 1997; Bourrelly et al. 2016). Gravity's influence on
88 oculomotor control should specifically affect visual perception, although weightlessness might

89 also induce distinct distortions in other sensory modalities. An alternative hypothesis is that
90 gravity does not affect visual signals *per se*, but rather affects an internal representation of space
91 (Clément et al., 2009, 2012), based on prior knowledge, that serves to interpret those signals,
92 independent of the sensory system from which they come (Wolbers et al., 2011; Loomis et al.,
93 2013). An example, among many, of the use of an internal model of space for perception is the
94 famous ‘Ames room’ illusion, where persons’ size is misperceived due to the use of the
95 inappropriate prior that the room is rectangular (O’Reilly et al., 2012). A direct implication of
96 this second hypothesis is that microgravity should distort all spatial perceptions in the same way,
97 regardless of the sensory modality. Because previous studies in microgravity were focused on
98 visual tasks only, however, these proposed hypotheses have never been tested.

99 To investigate these two assumptions, we first compared distortions of visual versus haptic
100 perception of 3D shape in a normal, upright posture on Earth. Next, we studied the effect of
101 changing the subject’s orientation with respect to gravity to assess whether any visual or haptic
102 distortions are egocentric or gravity-centric. Third, we tested the consequences of removing the
103 effects of gravity by performing both haptic and visual experiments in weightlessness during
104 parabolic flight.

105 **Materials and Methods**

106 In an analogy with previous experiments on visual perception (Clément et al., 2008, 2013), our
107 paradigm was conceptually designed to detect distortions in the perception of three-dimensional
108 shape, i.e., the relative lengths of the sides of a 3D cube. The sequential nature of haptic
109 perception induced us, however, to focus each trial on the comparison of the relative size between
110 two out of three possible dimensions. In both the visual and the haptic cases, the task consisted
111 of adjusting one side of the rectangle to match the other, to form a square. The adjustments were
112 performed using a trackball held in the left hand. In the haptic task the right hand was used to
113 explore the rectangle. Subjects pressed a button on a trackball when they perceived the object to
114 be perfectly square.

115 For the haptic tasks, subjects were asked to close their eyes and to feel, through haptic sense only,
116 a rectangular cutout in a rigid, virtual plank generated by a Force Dimension Omega.3 haptic

117 robot (Figure 1A). This manipulandum was able to simulate the presence of a 3D object by
118 applying the appropriate contact forces on the right hand of the subject when he/she performed
119 exploration movements aimed at perceiving its shape and size. During each trial the robot
120 constrained the subject's hand movement to lie within the plane of the virtual plank and to
121 remain inside the rectangle prescribed by the virtual cutout. To allow direct comparisons
122 between the experimental results from haptic and visual tests, an analogous bi-dimensional task
123 was also used for visual perception. Subjects were shown planar rectangles with different
124 orientations in 3D space, without being able to manually explore it. For trials involving visual
125 perception, an Oculus Rift virtual reality headset was used to provide a stereoscopic view of the
126 virtual object. The visual environment was dark and the shapes were represented by light-gray
127 frames. For both sensory conditions, the virtual object was located approximately 40 cm in front
128 of the subject's right shoulder.

129 Although there were no instructions to work quickly, subjects were asked to attempt to perform
130 each trial in a fixed time window (20 s for all experiments except those performed on board the
131 parabolic flight plane, for which a 10 s time window was used). An audible cue indicated to the
132 subject when the end of the allotted time was approaching. The apparatus recorded the subject's
133 final responses (dimensions of each rectangle judged to be square), which is the main output of
134 the tests. For the haptic tasks, the movements of the subject's hand and the contact forces applied
135 against the virtual constraints were also recorded via the haptic device.

136 The use of two-dimensional tasks allowed the estimation of the perceptive error in one plane at
137 a time. Subjects in our experiments judged the squareness of rectangles lying in each of three
138 anatomical planes: frontal, sagittal, or transversal (see bottom part of Figure 1A). The combination
139 of the three possible planes and the two rectangle dimensions resulted in six different geometric
140 configurations that the subject had to deal with. They are represented in the upper part of Figure
141 2. At the beginning of each trial, an audio command told the subject in which anatomical plane
142 the rectangle was lying and which of the two dimensions of the rectangle had to be adjusted. In
143 our paradigm, the reference dimension was always 40 mm, but subjects were not informed of this
144 fact. The initial length of the adjustable side was randomly selected between 15, 25, 35, 45, 55,
145 and 65 mm. Subjects performed five series of trials in all; each series being composed of a random

146 permutation of the six geometric configurations (total number of trials per condition: 30). In all
147 three experiments described below, each subject was tested in two different conditions, so that
148 in total each subject performed 60 trials. The two conditions, which depended on the experiment,
149 were tested successively and their order was counterbalanced (half of subjects started with
150 condition 1 and the other half with condition 2).

151

152

[Figure 1 about here]

153

154 **Experiment 1: Effect of Sensory Modality**

155 To study the differences and similarities between haptic and visual perception of 3D shapes in
156 normo-gravity, 18 seated subjects (8 males, 10 females, aged 29 ± 9) performed the task for all six
157 geometrical configurations in each of the two sensory conditions: Haptic and Visual. The order
158 of the two sensory conditions was randomized across subjects.

159 **Experiment 2: Effect of Body Orientation**

160 To study the perceptive distortions of both haptic and visual senses and whether the information
161 is encoded in an egocentric (body-centered) or allocentric (gravity-centered) reference frame, a
162 group of 18 subjects (9 males and 9 females, aged 25.5 ± 5 years) performed the haptic task while
163 seated (Upright) and while lying on the back (Supine), while a second group of 18 subjects (11
164 male and 7 female, aged 24 ± 4 years) performed the visual task in the same two postures (Upright
165 and Supine). For the Supine posture, subjects lied on a medical bed. The two postures are repre-
166 sented in Figure 2 together with the respective correspondence between egocentric and
167 allocentric references. The virtual object was placed always at the same distance from the subject's
168 shoulder, independent of the posture. In order to compensate for possible learning effects, the
169 order of the postural conditions was randomized in both sensory conditions.

170

171

[Figure 2 about here]

172

173 **Experiment 3: Effect of Weightlessness**

174 To study the role of gravitational cues in the encoding of haptic and visual signals we performed
175 the haptic (18 subjects: 10 males, 8 females, aged 38 ± 11 years) and visual (18 subjects: 9 males, 9
176 females, aged 41 ± 11 years) paradigm in normal gravity (1G) and during the weightlessness phases
177 of parabolic flight (0G). For the haptic experiment, a third condition was added: the subjects were
178 also tested in normal gravity, but with the arm supported by a strap (Supp.), to differentiate the
179 biomechanical effect of gravity on the arm from the gravitational stimulation of graviceptors,
180 such as the otoliths.

181 Parabolic flight provides short intervals (~20s) of weightlessness within a stable visual
182 environment inside the airplane, bracketed by periods of hyper-gravity (1.6 - 1.8 G) just before
183 and just after each period of weightlessness. Given the short duration of 0G phases during
184 parabolic flight, the subjects were trained to perform the task in about 10 seconds (two tasks per
185 parabola). Since each subject performed the experiment during 15 consecutive parabolas, he or
186 she could perform all 30 trials per condition.

187 All experimental conditions were performed inflight onboard the Novespace Zero-G airplane in
188 order to minimize possible undesired changes in uncontrolled factors. The 1G and Support
189 conditions were tested during the level-flight phase just preceding the first parabola or just
190 following the last parabola of its session, depending on the subject. The subjects were very firmly
191 restrained with belts so that their relative position with respect to the apparatus and the virtual
192 rectangles did not vary between gravitational conditions.

193 **Ethical approval**

194 The experimental protocols of experiment 1 and 2 performed at Université Paris Cité were
195 approved by the university review board "Comité Éthique de la Recherche" CER (approval
196 number 2016/33). The experiments performed on board of the Zero-G airplane were approved
197 by the French national ethic committee "Comité de Protection des Personnes", CPP (approval
198 number: 2014-A01949-38)

199 **Data analysis**

200 For each trial, t , the error, ε , between the length of the adjustable and reference sides of the
201 rectangle was computed. If the egocentered definition of the three dimensions (Lateral, LA ;
202 Longitudinal, LO ; Anterior-Posterior, AP) of Figure 1B is used, the errors of the six geometric
203 configurations are defined as $LA-LO$, $LO-LA$, $LA-AP$, $AP-LA$, $LO-AP$, and $AP-LO$, where the
204 minuend and subtrahend are the adjustable and reference dimensions respectively.

205

206 [Table 1 about here]

207

208 Table 1 shows how the perceptive distortion associated with each of the three dimensions
209 contributes to the error made on the six geometric configurations. Positive errors correspond to
210 underestimations of the adjustable dimension and/or to overestimations of the reference
211 dimension. Thus, the present experimental paradigm, similar to the one previously used by
212 Clément et al. (2008, 2013), allows the quantification of the perceptive errors of one dimension
213 relative to another, but cannot lead to a measure of the absolute perceptive errors for each
214 dimension separately.

215 ***Estimation of 3 orthogonal perceptual errors***

216 Table 1 shows that the error in estimating one dimension has opposite effects for the two tasks
217 performed within a given plane. For instance, an overestimation of the AP dimension should
218 result in negative and positive errors in the AP-LA and LA-AP tasks, respectively. These
219 relationships appear to be confirmed by the experimental results (Figure 4A), because this
220 hypothesis accounts for 96% of the data variance. It follows that the theoretical relationships
221 below are valid:

$$\begin{aligned}\varepsilon_{LA-AP} &= -\varepsilon_{AP-LA} \\ \varepsilon_{LA-LO} &= -\varepsilon_{LO-LA} \\ \varepsilon_{LO-AP} &= -\varepsilon_{AP-LO}\end{aligned}\tag{1}$$

222 Exploiting this property, it was possible to combine the five errors obtained for one geometric
 223 condition, with the additive inverse of the five errors obtained for the other geometric condition
 224 performed in the same plane. This allowed computing the combined mean and the variance of
 225 the errors for each of the three planes (Transverse, *Tra*; Frontal, *Fro*; Sagittal, *Sag*), instead of
 226 individually for each of the 6 geometrical configurations of the task. This technique has the
 227 considerable advantage of being more robust, because it is based on 10 samples instead of only 5.
 228

$$\begin{aligned}
 \bar{\varepsilon}_{Tra} &= \frac{\sum_{t=1}^5 (\varepsilon_{LA-AP,t} - \varepsilon_{AP-LA,t})}{10} \\
 \sigma_{Tra}^2 &= \frac{\sum_{t=1}^5 ((\varepsilon_{LA-AP,t} - \bar{\varepsilon}_{Tra})^2 + (-\varepsilon_{AP-LA,t} - \bar{\varepsilon}_{Tra})^2)}{10} \\
 \bar{\varepsilon}_{Fro} &= \frac{\sum_{t=1}^5 (\varepsilon_{LA-LO,t} - \varepsilon_{LO-LA,t})}{10} \\
 \sigma_{Fro}^2 &= \frac{\sum_{t=1}^5 ((\varepsilon_{LA-LO,t} - \bar{\varepsilon}_{Fro})^2 + (-\varepsilon_{LO-LA,t} - \bar{\varepsilon}_{Fro})^2)}{10} \\
 \bar{\varepsilon}_{Sag} &= \frac{\sum_{t=1}^5 (\varepsilon_{AP-LO,t} - \varepsilon_{LO-AP,t})}{10} \\
 \sigma_{Fro}^2 &= \frac{\sum_{t=1}^5 ((\varepsilon_{AP-LO,t} - \bar{\varepsilon}_{Sag})^2 + (-\varepsilon_{LO-AP,t} - \bar{\varepsilon}_{Fro})^2)}{10}
 \end{aligned} \tag{2}$$

229 With the above formulas, one can characterize perceptual distortions in each of the three
 230 different planes as illustrated in Figure 3. By our convention, a rectangle lying in one of the two
 231 vertical planes (Sagittal or Frontal) is associated with a positive error (stubby rectangle) if the
 232 longitudinal dimension is smaller than the other dimension. In the transverse plane, a positive
 233 error (stubby rectangle) corresponds to the AP dimension being smaller than the LA dimension.
 234 It is worth noting that if the subject produced a “stubby” rectangle (positive errors) this means
 235 that he/she perceived a square to be “slender”, and vice versa. The global variance was computed
 236 as the average of the three planar variances.

237

238

[Figure 3 about here]

239

240 The estimation of the three planar errors is then improved by considering that if the (distorted)
241 metrics used to compare distances in 3D space are locally smooth and consistent for the different
242 dimensions in space, the three planar errors ε are not independent and that, given the sign
243 conventions of Figure 3, they should fulfill the following relationship

$$\bar{\varepsilon}_{Sag} + \bar{\varepsilon}_{Tra} = \bar{\varepsilon}_{Fro} \quad (3)$$

244 Note that equation 3 is a particular case of the formula describing a plane, $ax + by + cz = d$, where
245 $a = b = 1$, $c = -1$ and $d = 0$. Thus, if the metrics in each plane are consistent with each other, the
246 vectors of measured planar errors $\bar{\varepsilon} = [\bar{\varepsilon}_{Sag} \ \bar{\varepsilon}_{Tra} \ \bar{\varepsilon}_{Fro}]$ should fall on that plane and points outside
247 the plane can be considered to be noise. By projecting the individual vectors $\bar{\varepsilon}$ onto the plane
248 corresponding to equation 3 as shown in Figure 4A-B, this noise is effectively filtered out. Using
249 the resulting 2D representation of the distortion (Figure 4C) is a conservative choice, especially
250 when comparing their orientation in different conditions, because the 3D representation may
251 lead to consider distortion directions and components of data variability that have no functional
252 meaning. On average, the data projected on the plane of equation 3 account for 98% of the
253 variance of the original data, suggesting that the recorded responses tend to well fulfill this
254 constraint.

255

256

[Figure 4 about here]

257

258 We used the same equations (1-3) to compute the analogous parameter in the allocentric
259 reference frame after having replaced the egocentrically defined planes and directions with the
260 world-centered planes (Horizontal, *Hor*; Latitudinal, *Lat*; Meridian, *Mer*) and directions (*East-*
261 *West*, *North-South*, and *Up-Down*) as shown in Figure 2. Table 2 shows the relationships
262 between the planar distortions defined in the body-centered and gravity-centered reference
263 frame for the Upright and Supine posture.

264

265

[Table 2 about here]

266

267 **Perceptive cuboids**

268 Although, as stated before, the present experimental paradigm, does not allow a measure of the
 269 absolute perceptive errors for each dimension separately, we have devised a methodology that
 270 allows one to visualize the 3D patterns of distortion as a “perceptive cuboid”, that is an elongated
 271 box compared to an ideal undistorted cube. To compute the dimensional errors, we first solved
 272 the system of equations of Table 1 reported below in the matrix form.

$$273 \begin{bmatrix} \varepsilon_{LA-LO} \\ \varepsilon_{LO-LA} \\ \varepsilon_{LA-AP} \\ \varepsilon_{AP-LA} \\ \varepsilon_{LO-AP} \\ \varepsilon_{AP-LO} \end{bmatrix} = A \cdot \begin{bmatrix} \varepsilon_{LA} \\ \varepsilon_{AP} \\ \varepsilon_{LO} \end{bmatrix} = \begin{bmatrix} 1 & 0 & -1 \\ -1 & 0 & 1 \\ 1 & -1 & 0 \\ -1 & 1 & 0 \\ 0 & -1 & 1 \\ 0 & 1 & -1 \end{bmatrix} \cdot \begin{bmatrix} \varepsilon_{LA} \\ \varepsilon_{AP} \\ \varepsilon_{LO} \end{bmatrix}$$

274 If we call A the matrix of linear coefficient, then the solutions of this underdetermined problem
 275 are

$$276 \begin{bmatrix} \varepsilon_{LA} \\ \varepsilon_{AP} \\ \varepsilon_{LO} \end{bmatrix} = A^\dagger \cdot \begin{bmatrix} \varepsilon_{LA-LO} \\ \varepsilon_{LO-LA} \\ \varepsilon_{LA-AP} \\ \varepsilon_{AP-LA} \\ \varepsilon_{LO-AP} \\ \varepsilon_{AP-LO} \end{bmatrix} + (I - A^\dagger A) * \begin{bmatrix} \varepsilon_{LA} \\ \varepsilon_{AP} \\ \varepsilon_{LO} \end{bmatrix} = A^\dagger \cdot \begin{bmatrix} \varepsilon_{LA-LO} \\ \varepsilon_{LO-LA} \\ \varepsilon_{LA-AP} \\ \varepsilon_{AP-LA} \\ \varepsilon_{LO-AP} \\ \varepsilon_{AP-LO} \end{bmatrix} + (I - A^\dagger A)w = A^\dagger \cdot \begin{bmatrix} \varepsilon_{LA-LO} \\ \varepsilon_{LO-LA} \\ \varepsilon_{LA-AP} \\ \varepsilon_{AP-LA} \\ \varepsilon_{LO-AP} \\ \varepsilon_{AP-LO} \end{bmatrix} + \begin{bmatrix} w \\ w \\ w \end{bmatrix}$$

277 Where the A^\dagger is the pseudo inverse of A and w is a free scalar parameter that reflects the fact that
 278 the observed results can be explained by an infinity of triplets of dimensional distortions differing
 279 by isotropic component, w , only (underdetermination of the problem).

280 To define a set of dimensional errors, $(\varepsilon_{LA}, \varepsilon_{AP}, \varepsilon_{LO})$ to be used for a graphical representation, we
 281 arbitrary decided to select the solution that minimizes the Euclidean norm of the error vectors.

282 Although the w parameter cannot be univocally defined, the difference between the errors along
 283 the three dimensions are correctly quantified and then used to test the anisotropy of the
 284 perceptive errors. The dimensional errors, however, cannot be rigorously compared between
 285 postures or gravitational conditions, because the differences between experimental conditions
 286 could be due to differences in defining the w parameter for each condition.

287 ***Polar representation of errors***

288 The 2D vector resulting from the projection of $\bar{\epsilon}$ to the plane of equation 3 was computed for
289 each subject (Figure 4C) and represented with a polar plot. The vector length corresponds to the
290 Euclidian sum of the filtered error triplets and its direction provides information about the
291 “shape” of the pattern of errors, meaning the relative magnitude and sign of the errors in the
292 three anatomical planes: a pattern of errors restricted to an expansion or contraction along the
293 anterior-posterior axis, with no errors in the fronto-parallel plane will give a vector pointing
294 along the 0° or 180° axes, respectively; a pattern of errors restricted to a contraction or expansion
295 along the lateral axis, with no errors in the sagittal plane corresponds to a vector with a 60° or
296 240° orientation, respectively; a pattern of errors that is restricted to an expansion or contraction
297 in the longitudinal direction, with no distortion between the axes in the transversal plane will
298 give a vector that points along the 120° or 300° axes in the polar plot, respectively. Vectors that
299 point along intermediate angles indicate more complex patterns wherein an over-estimation
300 along one anatomical axis and an underestimation along another axis are combined (e.g. the 30°
301 orientation corresponds to AP and LA dimensions that are respectively over-estimated and
302 underestimated compared to LO).

303 The strength of the misalignment, *Mis*, between the individual 2D vectors representing the two
304 conditions tested in an experiment, was computed as the cross-product of the two individual
305 vectors. The value of *Mis*, which, as illustrated in Figure 4D, corresponds to the area of the
306 parallelogram having the two vectors as adjacent sides, is zero when the two vectors are in the
307 same, or opposite, direction and maximal when they are orthogonal. Importantly, *Mis* amplitude
308 depends also on the vectors’ lengths, so that the *Mis* value associated to long vectors is larger than
309 for short vectors for the same amount of misalignment. This gives a desired feature that large
310 vectors, which have a well-defined direction, are given greater weight in statistical analyses than
311 small vectors whose direction can be significantly deviated by experimental noise.

312 In each experimental condition, the vectorial mean of the 2D individual vectors was computed
313 to represent the average perceptive error.

314 **Reaction forces during haptic task**

315 To estimate changes of the contact forces between gravitational conditions in the haptic tasks,
316 we computed the average of the reaction forces generated by the haptic device when the subject's
317 hand was in contact with the edges of the virtual cutout or when the hand tried to move out of
318 the task plane.

319 **Microgravity effect and theoretical prediction**

320 To quantify the effect of microgravity on the perceptive errors, for each subject, s , the mean
321 planar error in 1G was subtracted from the corresponding error in 0G:

322
$$\Delta\bar{\epsilon}_s = \bar{\epsilon}_{s,0G} - \bar{\epsilon}_{s,1G}$$

323 To predict the perceptive distortion expected in microgravity under the hypothesis that the 0G
324 effect was identical for the haptic and visual modalities, we averaged all error triplets $\Delta\bar{\epsilon}_s$
325 representing the measured individual microgravity effects from both the haptic and visual
326 experiments (18 haptic subjects, 18 visual subjects):

327
$$\Delta\bar{\epsilon} = \frac{\sum_{s=1}^{36} \Delta\bar{\epsilon}_s}{36}$$

328 The obtained average triplet was then added to the individual visual and haptic errors measured
329 in normo-gravity conditions to compute the predicted error in microgravity, $\hat{\epsilon}_{s,0G}$.

330
$$\hat{\epsilon}_{s,0G} = \bar{\epsilon}_{s,1G} + \Delta\bar{\epsilon}$$

331 We then compared these individual predictions to the errors measured in 0G for both visual and
332 haptic modalities, to see to what extent a common mechanism for visual and haptic captures the
333 data.

334 **Statistical analysis**

335 For each experiment, we first tested the significance of the squaring errors by testing for each
336 plane whether the constant errors were on average different from zero (two-sided Student's t-
337 test). Then, we performed repeated-measures ANOVA on the constant and variable errors. The
338 sign conventions (Figure 3) being arbitrary, they allow a rigorous comparison of the errors within
339 a given plane, but they do not allow the comparison between different planes. For this reason, in

340 the statistical analyses, the results on each plane were tested with independent ANOVAs for
341 repeated measures.

342 Experiment 1: For each of the 3 task planes we tested for an effect of Sensory Modality on the
343 perceptive error as a single within-subject independent factor with two levels (Haptic, Visual).

344 Experiment 2: We tested for an effect of Body Posture as a within-subject independent factor
345 with two levels (*Upright*, *Supine*) in separate ANOVAs for each group/sensory modality (Visual
346 and Haptic). Note that this separation is justified by the hypotheses being tested, for which cross
347 effects between posture and modality would have little meaning. To test whether errors are tied
348 to a body-centric or gravity-centric reference frame, we defined the task planes both in terms of
349 anatomical axes and world axes. Invariance of pattern of error (lack of a statistical difference) for
350 the anatomically defined planes, but not the world-defined frames, would indicate that the errors
351 are primarily egocentrically, rather than allocentrically, aligned.

352 Experiment 3: For each of the 3 task planes we tested for an effect of Gravity on the squaring
353 error as a single within-subject independent factor with three (1G, 0G, Supported) and two (1G,
354 0G) levels for the haptic and visual experiment respectively.

355

356 Before performing each ANOVA, we tested for normality and homogeneity of the distributions
357 using the Kolmogorov-Smirnov and Levenes tests, respectively. To achieve the normal
358 distribution for the response variability, the standard deviations were transformed by the
359 $\log(\sigma+1)$ function (Tagliabue and McIntyre 2011). For the errors expressed in both allocentric
360 and egocentric reference frames the data were distributed normally (all $p>0.20$) and the data
361 variability was similar among all conditions (all $p>0.50$).

362 In order to test whether the variability of the individual squaring errors in the haptic modality
363 can explain the errors in the visual modality (and vice versa), their coefficient of correlation R ,
364 with the relative p-value, was computed.

365 Because the *Mis* parameter did not always show a normal distribution, it is presented in terms of
366 median \pm inter-quartile range and a non-parametric Sign Test was used to test whether its
367 distribution is significantly different from zero.

368 To test whether the pattern of errors (2D vectors) differs between two conditions (experiment 1:
369 visual vs haptic; experiments 2: upright vs supine; experiments 3: 1G vs 0G), a bootstrap technique
370 was used. This technique, which allows one to correctly take into account both direction and
371 amplitude of the individual vectors, consisted of using 10000 re-samplings with replacement of
372 the 18 subjects to estimate the statistical distribution of the difference in amplitude, ΔAmp , and
373 the angle, θ , between the vectorial average of two conditions, and to compute the probability of
374 error in rejecting the null hypothesis, H_0 , that $\theta=0$. Following a Bayesian approach, taking into
375 account a prior uniform distribution of all possible angles (θ range $\pm 180^\circ$), we evaluated the ratio,
376 $R_{0/1}$, between the probability to obtain the observed data under the null hypothesis, H_0 , and the
377 probability under the alternative hypothesis, H_1 , that $\theta \neq 0$ (Wagenmakers et al., 2018).

378 In experiment 3, to test whether the effect of microgravity has the same direction for visual and
379 haptic modalities the bootstrap re-sampling was performed independently for the two sensory
380 conditions, because different groups of subjects were tested for the two modalities.

381

382 Results

383 Experiment 1: Haptic and Visual Perception

384 Figure 5A shows that for the six geometric configurations of the squaring task (see methods) the
385 subjects made systematic errors in both visual and haptic conditions. The comparison of the errors
386 made using haptic information alone versus visual information alone shows consistent, opposing
387 results for the two sensory modalities. Hence, in each task, when subjects made on average
388 significant positive errors in the haptic condition, they made negative errors in the visual
389 condition, and vice versa. Figure 5B represents the more robust evaluation of the errors obtained
390 by considering the constraints existing between the errors performed in the six squaring tasks
391 (see Methods, equations 1-3). The amplitude of the error was significantly different from zero for
392 both visual and haptic perception in the Sagittal (visual: $F_{(17)}=5.86$, $p<10^{-4}$, haptic: $F_{(17)}=-8.10$, $p<10^{-6}$)
393 and Transversal plane (visual: $F_{(17)}=-7.22$, $p<10^{-5}$, haptic: $F_{(17)}=9.22$, $p<10^{-6}$), but in the Frontal
394 plane neither modality was significantly different from zero (visual: $F_{(17)}=-1.26$, $p=0.22$, haptic
395 $F_{(17)}=-0.57$, $p=0.58$). Sensory modality had a significant effect in the Sagittal ($F_{(1,17)}=60.8$, $p<10^{-5}$)

396 and Transversal ($F_{(1,17)}=94.96$, $p<10^{-6}$) planes, but not in the Frontal plane ($F_{(1,17)}=0.14$, $p=0.71$).
397 Remarkably, the significant perceptive errors in the Sagittal and Transversal planes had opposite
398 sign between the two sensory conditions: when using haptic sense, subjects produced rectangles
399 with the Anterior-Posterior dimension smaller than the Longitudinal and Lateral dimension,
400 while, when using vision, they made rectangles with the Anterior-Posterior dimension larger
401 than the Longitudinal and Lateral dimension. Moreover, when looking at the individual error in
402 Figure 5C a strong (negative) correlation can be observed between visual and haptic errors ($R=-$
403 0.79 , $p<10^{-12}$), showing a clear relationship between the two, meaning that subjects who showed
404 a stronger distortion in the visual domain also showed a stronger distortion, but in the opposite
405 direction, in the haptic domain. The correlation remained significant when the average error in
406 each plane was subtracted from the corresponding individual values (insert of Figure 5C, $R=-0.28$,
407 $p<0.05$).

408 The vectorial representation of the individual errors for the two sensory modalities in Figure 5D
409 fall along the same axis, but in opposite directions, meaning that the perceptual errors were in
410 both cases restricted to an expansion (haptic) or contraction (visual) along the antero-posterior
411 axis with little or no distortion in the fronto-parallel plane. The pattern of errors for the two
412 modalities appear therefore complementary, in that they would tend to mutually cancel out when
413 combined. Consistently, the analysis of cross-product between the haptic and visual individual
414 vectors does not reveal any significant misalignment ($Mis=-52\pm 55\text{mm}^2$, signed test: $p=0.48$). The
415 angle θ between the average visual and haptic vector is $172\pm 6^\circ$ and not significantly different
416 from 180° (bootstrap $p=0.07$). Taking into account all possible orientations for the two groups of
417 vectors, the observed results are 9 times more likely under the hypothesis that pattern of errors
418 of the two senses are complementary ($H_0: \theta=180^\circ$), than under the alternative hypothesis (H_1), i.e.
419 $\theta\neq 180^\circ$. The average visual and haptic vectors show, on the other hand, amplitudes that are
420 significantly different (bootstrap: $\Delta Amp=5.8\pm 2\text{ mm}$ $p=0.003$), meaning that, although the pattern
421 of errors for the two modalities are complementary, they would not exactly cancel each other
422 out, although the difference would be small. The illustration of the 'perceptive cuboids'
423 corresponding to the two sensory modalities reported in Figure 5E confirms that the haptic and

424 visual perceptive errors would mainly consist of a depth overestimation and underestimation for
425 the haptic and visual sense, respectively.

426 Even though the amplitude of the perceptive biases (constant components of the errors reported
427 in Figure 5) appear smaller for the haptic than for the visual modality, the latter is characterized
428 by a clearly smaller intra-personal variability of the responses ($\sigma_{\text{hapt}}=6.1\pm 2.6$ mm, $\sigma_{\text{vis}}=4.2\pm 2.2$ mm,
429 sensory modality effect: $F_{(1,17)}=12.02$, $p<10^{-2}$), corresponding to a higher precision for the visual
430 than for the haptic task.

431

432 [Figure 5 about here]

433

434 In summary, Experiment 1 shows clear differences in the patterns of visual and haptic distortions.
435 For both modalities the errors appeared primarily in the sagittal and transversal planes, and
436 amplitude and sign of the errors in one modality depended on amplitude and sign of the errors in
437 the other modality. More precisely, the pattern errors were opposite (contraction and expansion
438 of perceived depth for visual and haptic, respectively).

439

440 **Experiment 2: Effect of Body Orientation**

441 The responses of the subjects upright were characterized by constant errors similar to those
442 observed in Experiment 1 (Experiment effect: Wilks' Lambda=0.85, $F_{(4,32)}=1.35$, $p=0.27$). The left
443 columns of Table 3 and left panels of Figure 6 show that for both haptic and visual experiments
444 the squaring error appears consistent between postures if expressed egocentrically: we observed
445 no statistically significant effects of posture on the errors for any of the three planes when
446 expressed in body-centered reference frame. The misalignment, Mis , between the individual
447 vectors corresponding to upright and supine conditions (lower-left part of Figure 6A and 6B) is
448 not significantly different from zero (haptic: $Mis=20\pm 47$ mm², signed test $p=0.81$; vision:
449 $Mis=2\pm 12$ mm², signed test: $p=1$). For both sensory modalities, the difference in amplitude and
450 direction between average vector representing the pattern of errors in the upright and supine

451 position do not differ significantly from zero (bootstrap for haptics: $\Delta Amp=0.1\pm 1.1$ mm $p=0.56$,
452 $\theta=6\pm 14^\circ$ $p=0.33$, $R_{0/1}=9.3$; bootstrap for vision: $\Delta Amp=-2\pm 1.5$ mm $p=0.09$, $\theta=2\pm 3^\circ$ $p=0.25$; $R_{0/1}=38$).

453 On the other hand, if the errors are represented in terms of allocentrically defined planes, i.e.
454 fixed with respect to gravity (last three columns of Table 3 and right panels of Figure 6), a clear
455 effect of posture can be observed in all planes for both sensory modalities on the orientation of
456 the pattern of errors with significant misalignments: haptic $Mis=38\pm 19$ mm² signed test: $p=0.007$;
457 vision: $Mis=109\pm 55$ mm² signed test: $p=0.001$). Consistently, the angle between the average
458 vectors representing the errors in the allocentric space for the two postures is significantly
459 different for both modalities: bootstrap $p<10^{-4}$ for haptics and vision.

460

461 [Figure 6 about here]

462 [Table 3 about here]

463

464

465 The intra-personal variability of the responses was not affected by the posture for the haptic
466 modality ($\sigma_{upright}=6.2\pm 6.1$ mm, $\sigma_{supine}=6.6\pm 6.0$ mm, posture effect: $F_{(1,17)}=0.12$, $p=0.73$), but
467 significantly increased in the supine position for the visual experiment ($\sigma_{upright}=3.5\pm 3.2$ mm,
468 $\sigma_{supine}=4.8\pm 4.7$ mm, posture effect: $F_{(1,17)}=6.81$, $p=0.02$).

469 In conclusion, in this experiment we found that patterns of errors of both visual and haptic
470 perception were invariant when expressed in an egocentric reference frame, but not when
471 expressed in an allocentric one.

472 **Experiment 3: Gravity's Effect on Visual and Haptic Perception**

473 While the visual inputs are not different on ground and in weightlessness, the forces exerted
474 against the virtual constraints during haptic exploration might be different in 0G due to
475 biomechanical and neurophysiological effects. We therefore first analyze the changes in the
476 contact forces between the subject's hand and the virtual object and then the pattern of squaring
477 errors (Figure 7A-C). The left plot of Figure 7A shows that vertical forces applied by the subjects

478 on the upper and lower edge of the sensed object were modulated ($F_{(2,34)}=3.9$, $p=0.02$) by the
479 experimental conditions (1G, 0G, Supported). As expected, upward and downward forces
480 increased and decreased respectively in microgravity (post-hoc 1G Vs 0G, $p=0.02$), coherent with
481 a reduction of the weight of the upper limb. When the weight of the arm was supported (see
482 methods), the vertical forces also tended to differ from 1G condition (post-hoc Supp Vs 1G
483 $p=0.09$) and were modulated in the same direction as in 0G (post-hoc Supp Vs 0G, $p=0.29$).
484 Horizontal forces were also significantly affected by the experimental condition ($F_{(2,34)}=6.32$,
485 $p<0.01$; Figure 7A, right plot), with a significant increase of the contact forces in microgravity
486 with respect to the 1G and Support conditions.

487 This increase of the contact force in 0G, similar to what was previously observed in haptic tests
488 during parabolic flights (Mierau et al., 2008), could be the result of a specific strategy aimed at
489 keeping muscular tension, and hence muscle spindle sensitivity, similar to normal gravity
490 conditions. This strategy would avoid the decrease in proprioception precision previously
491 observed in weightlessness for 'open-chain' motor tasks, for which the same strategy could not
492 be adopted, resulting in a decrease in muscle tension (Clément and Reschke, 2010). This
493 hypothesis well matches the fact that the precision of haptic responses was not significantly
494 affected by the experimental condition (response variability: 1G 6.8 ± 2.6 , 0G 7.1 ± 3.1 , Sup 6.4 ± 2.9 ;
495 $F_{(2,34)}=1.75$, $p=0.19$), suggesting that neither microgravity nor the arm support significantly
496 interfered with the subjects' ability to perform the task. This lack of microgravity effect on haptic
497 precision appears in line with the results of previous orbital experiments (McIntyre and Lipshits,
498 2008).

499 Importantly, the results about the vertical contact forces and responses' variability suggest that
500 the 'arm support' condition successfully mimicked the expected lightening of the arm observed
501 in microgravity. Therefore, if haptic perceptive distortions (constant errors) are affected by
502 microgravity, but not by the arm support, they would not be directly ascribable to the
503 biomechanical action of microgravity on the arm.

504

505

[Figure 7 about here]

506

507 The comparison of the constant errors in the three experimental conditions, reported in Figure
508 7B, clearly shows that the perceptive distortion characterizing haptic perception in the Sagittal
509 plane was significantly amplified (became more negative) by microgravity, but was not affected
510 by the arm support (condition effect $F_{(2,34)}=12.49$, $p<10^{-4}$), suggesting a perceptive rather than
511 biomechanical effect. Similarly, the haptic distortion in the Transversal plane was amplified
512 (became more positive) in 0G and was not affected by the support, either (condition effect
513 $F_{(2,34)}=11.13$, $p<10^{-3}$). Finally, the lack of distortion in the Frontal plane persisted independent of
514 the gravitational and support condition ($F_{(2,34)}=0.33$, $p=0.71$). Figure 7C shows a clear increase of
515 the amplitude of average error vector in 0G (bootstrap: $\Delta Amp=5\pm 1$ mm, $p<10^{-4}$). A nonsignificant
516 misalignment between the haptic individual errors in the two gravitational conditions is reported
517 ($Mis=2\pm 33$ mm², signed test $p=1$) and consistently, the angle θ between the two average vectors
518 is not significantly different from 0 (bootstrap $-5\pm 16^\circ$ $p=0.62$; $R_{0/1}=8.4$).

519 For the visual tasks, Figure 7D shows that, as for the haptic sense, microgravity significantly
520 modulated the perceptive distortions. More precisely, the large errors characterizing both sagittal
521 and transversal planes in 1G were significantly reduced in weightlessness ($F_{(1,17)}=15.41$, $p=0.0011$
522 and $F_{(1,17)}=7.87$, $p=0.012$ respectively). In the frontal plane, a small but significant height
523 underestimation appeared in 0G ($F_{(1,17)}=9.531$, $p=0.007$). The polar plot of Figure 7E shows that
524 the amplitude of the average error vector decreases in microgravity (bootstrap $\Delta Amp=-2.8\pm 0.8$
525 $p<10^{-4}$). Note that there is a small but significant misalignment between the 1G and 0G vectors
526 ($Mis=16\pm 12$, signed test $p=0.007$, bootstrap $\theta=7\pm 3^\circ$ $p<10^{-4}$). The analysis of the variable component
527 of the errors shows that microgravity did not significantly affect subjects' visual precision
528 ($F_{(1,17)}=4.3$, $p=0.054$), although the response variability tended to increase from 4.4 ± 2.5 to 5.2 ± 2.4
529 mm.

530 The qualitative comparison of Figure 7F and Figure 7G illustrates that the effect of gravity on
531 both sensory modalities mainly consists of a stretch of depth perception with respect to normo-
532 gravity conditions (an increase in slenderness for haptic; a decrease in stubbiness for visual).

533 In neither haptic nor visual 0G tasks did the amplitude of the errors appear to change over the
534 parabolas (trial number effect on haptic errors: Sagittal $F_{(4,60)}=0.79$, $p=0.54$; Transversal $F_{(4,60)}=0.23$,
535 $p=0.92$; Frontal $F_{(4,60)}=0.49$, $p=0.74$; and on visual errors Sagittal $F_{(4,68)}=1.23$, $p=0.30$; Transversal
536 $F_{(4,68)}=0.60$, $p=0.67$; Frontal $F_{(4,68)}=0.63$, $p=0.64$) suggesting a lack of significant adaptation to
537 microgravity during the experiment duration.

538 The direct quantitative comparison of the effect of microgravity, $\Delta\bar{\epsilon}_s$, between the two groups of
539 subjects of the visual and haptic experiments (Figure 8A) shows similar modulations of the
540 perceptual distortion for both senses (Wilks' Lambda=0.91, $F_{(3,32)}=0.96$, $p=0.42$). Although
541 the amplitude of the microgravity effect tends to be larger for haptic than for visual perception
542 (bootstrap, $p=0.06$), the average directions of the microgravity effect on visual and haptic
543 sense appear very similar (Figure 8B): the angle θ between the two vectors representing
544 the average effect of gravity on the two modalities is only $15.6\pm 15.6^\circ$ and not significantly
545 larger than zero (bootstrap, $p=0.14$). When considering the range of all possible θ ($\pm 180^\circ$),
546 Bayesian statistics suggest that the observed data are 5.2 times more likely under the
547 hypothesis that $\theta=0^\circ$ (H_0) than under the hypothesis $\theta\neq 0^\circ$ (H_1). As shown in Figure 7B and
548 7D, the perceptive error predicted in 0G, $\hat{\epsilon}_{s,0G}$, by assuming that the gravity effect is identical for
549 the haptic and visual modality (both in terms of direction and amplitude) are indeed
550 indistinguishable from the observed results (Wilks' Lambda=0.73, $F_{(6,12)}=0.73$, $p=0.63$), despite the
551 small difference in orientation between $\Delta\epsilon_{visual}$ and $\Delta\epsilon_{haptic}$ and despite the slight change in
552 orientation of the visual vector when passing from 1G to 0G (see above).

553

554 [Figure 8 about here]

555

556 To summarize, the parabolic flight experiments show that, although opposite perceptive errors
557 characterize vision and haptic sense in normal gravity conditions, the effects of microgravity on
558 each of those patterns of errors are in the same direction for the two sensory modalities.

559 Results Summary

560 Experiment 1 revealed strong, complementary distortions between haptic and visual perception
561 of 3D geometry. Subjects visually underestimated an object's depth with respect to both height

562 and width, whilst overestimating depth when exploring the object haptically. In Experiment 2
563 the comparison of seated versus supine body orientation clearly showed that both visual and
564 haptic distortions align with the subject's body rather than with gravity. Experiment 3, conducted
565 during parabolic flight, showed a clear effect of microgravity on both haptic and visual distortion.
566 Importantly, despite the fact that the perceptive errors in normo-gravity were in the opposite
567 directions for visual and haptic tasks, the changes induced by microgravity were in the same
568 direction along the anterior-posterior axis: weightlessness increases the haptic over-estimation of
569 depth with respect to width and height and decreases the visual under-estimation of depth with
570 respect to width and height.

571 **Discussion**

572 The experiments presented here aimed to understand how gravity affects the perception of 3D
573 shapes. We extend previous studies restricted to vision to include haptic sensation, by using the
574 same experimental paradigm for the two modalities. In the following we argue for a modality-
575 independent role of gravity in interpreting incoming sensory signals.

576 **Haptic and Visual perception in normo-gravity conditions**

577 Individually, the visual and haptic distortions observed here are consistent with previous findings
578 obtained without using head-mounted displays or haptic devices, supporting the validity of the
579 present experimental paradigms. Our haptic results concur with overestimation in the radial
580 dimension observed for haptic tasks (Lipshits et al., 1994; Armstrong and Marks, 1999; Fasse et
581 al., 2000; Henriques and Soetching, 2003). Similarly, visual underestimation of depth has been
582 previously reported in the horizontal plane (Wagner, 1985; Loomis and Philbeck, 1999).
583 Surprisingly, we observed no significant 'horizontal-vertical illusion' previously observed in the
584 frontal plane (Avery and Day, 1969). Stimulus placement in front of the right shoulder in our
585 experiment, rather than straight ahead, may have impeded interpreting vertical and horizontal
586 lines as depth cues, which is purported to be the source of the illusion cited here (Girgus and
587 Coren, 1975).

588 Our experiments with supine subjects also show that the patterns of visual and haptic errors are
589 tied to the axes of the body, not to gravity. Although in apparent contradiction with the effects
590 of body tilt on visual tasks (Marendaz et al., 1993; Leone, 1998; Barnett-Cowan et al., 2015), or
591 external forces on haptic perception (Wydoodt et al., 2006), our observed posture-invariant error
592 pattern concurs with previously reported body-centered and eye-centered encoding of haptic
593 (Gurfinkel et al., 1993; Dupin et al., 2018) and visual information (Averly and Day, 1969; Howard
594 et al., 1990; McIntyre et al., 1997; Henriques et al., 1998; Vetter et al., 1999) and with the lack of
595 body-tilt effect in unimodal, but not cross-modal, tasks (Bernard-Espina et al., 2022).

596 Although perceptual biases are already known to differ between visually and haptically guided
597 pointing (vanBeers et al., 1999; Liu et al., 2018), we show for the first time a complementarity
598 and a negative correlation between the two. Although we cannot fully discard the hypothesis of
599 a fortuitous correspondence between modality-specific mechanisms, such as integration of eye
600 vergence signals for vision (Murdison et al., 2019) or exploratory movement kinematics for haptic
601 (Armstrong and Marks, 1999), our findings suggest some level of shared neural processing. In
602 previous studies, the sequential nature of haptic shape exploration, requiring information storage
603 in working memory, was shown to contribute to perceptive distortions (McFarland & Soechting,
604 2007). Similarly, both pointing to memorized targets (McIntyre et al., 1998) and haptic-visual
605 comparisons (McIntyre and Lipshits, 2008) showed distortions related to memory storage and
606 coordinate transformations. The sequential nature of the haptic explorations in our experiments,
607 and the likely need for sequential visual scanning, plus the need to compare lengths along
608 different directions, would require similar central processing of spatial information. The clearly
609 different distortions in visual versus haptic suggests that these tasks are carried out by separate,
610 modality-specific processes. Nevertheless, the link between modality-specific squaring errors
611 reported here suggests that central neural processes associated with memory storage and
612 coordinate transformations are shared between the two.

613

614 **3D object perception in microgravity**

615 Although the egocentric patterns observed for visual and haptic errors would suggest that an
616 external cue, such as gravity, should not influence shape perception, the strong microgravity
617 effects observed in parabolic-flight clearly show the contrary. How can these apparently
618 contradictory results be reconciled? We have shown that the observed effects of microgravity on
619 both haptic and visual perceptive distortions are not directly ascribable to a decrease in their
620 precision, nor to the mechanical action of gravity on the arm in the haptic task (arm support and
621 supine conditions). Moreover, the remarkable similarity between microgravity's effects on visual
622 and haptic distortions makes it unlikely that they are caused by independent effects on the two
623 sensory systems, such as modifications of proprioceptive-tactile receptors' output for haptic tasks
624 (Lipshits et al., 1994) or alterations of eye movement control for visual tests (Clement et al., 1989;
625 Clarke et al., 2013). A more parsimonious and likely explanation is an effect of gravity on sensory
626 processing that is shared by the two sensory modalities, which could be only hypothesized in
627 previous unimodal studies (Clement et al. 2009, 2012, 2013).

628 **Through what mechanism does gravity affect shape perception?**

629 The observed modality-independent effects of gravity on shape perception can be associated to
630 vestibular/otolithic projections toward the neural-network that recurrently connect the brain
631 areas involved in the haptic and visual representation of objects and whose existence has been
632 revealed by various brain imaging and electrophysiological studies (Figure 9A). The Lateral
633 Occipital Complex (LOC), known to be activated by 3D object images, is also active during haptic
634 shape recognition. Similarly, S1, S2, vPM and BA5 areas, commonly associated with haptic object
635 perception are activated also by images of manipulable objects. These cross-modal activations are
636 mediated by the intraparietal sulcus (IPS), whose activity is enhanced during cross-modal, visuo-
637 haptic object recognition. That IPS plays a role in reconstructing a visual representation of a
638 haptically sensed object, and vice versa, is supported by electrophysiological activity consistent
639 with recurrent neural networks able to perform cross-modal sensory re-encoding (Pouget et al.,
640 2002; Avillac et al., 2005). The coexistence of visual and haptic object representations, as depicted
641 in Figure 9B, is consistent with behaviourally observed concurrent representations of

642 reaching/grasping tasks (McGuire and Sabes, 2009, 2011; Tagliabue and McIntyre, 2011-2014)
643 and with the link that we observed here between haptic and visual perceptive errors in normo-
644 gravity conditions.

645 [Figure 9 about here]

646 We propose the trans-modal processing performed by IPS, as depicted in Figure 9, as the source
647 of the modality-independent distortions observed when performing the experiment in 0G. To
648 transform a visually-acquired object into a stable haptic representation (and vice versa), despite
649 potential independent movements of the two sensory systems, the IPS network must use a stable
650 internal representation of the body and/or peripersonal space (Andersen et al., 1997; Cohen and
651 Andersen, 2002; Land, 2014), built by constantly integrating signals about the eye-hand
652 kinematic chain and the body position in space, including vestibular inputs. Clear evidence that
653 internal models of body/space affect the interpretation of incoming sensory information in a
654 Bayesian fashion has been extensively reported, e.g. the 'Ames room' and the Müller-Lyer visual
655 illusions being based on prior knowledge about the geometry of constructed environments
656 (O'Reilly et al., 2012) or the cutaneous Rabbit illusion (Goldreich et al., 2007). The contribution
657 of gravitational signal to the body/space representation concurs with a) vestibular (i.e. otolithic)
658 projections to IPS-area reported in numerous electrophysiological studies (Blanke et al., 2000;
659 Miyamoto et al., 2007; Schlindwein et al., 2008; Chen et al., 2011, 2013), b) the observed
660 interference of head-tilt with the re-encoding of sensory signals between visual and haptic space
661 (Tagliabue and McIntyre, 2011, 2013; Burns et al., 2011; Bernard-Espina et al., 2022) and c) the
662 effect of vestibular stimulation on self-body-size perception (Mast et al., 2014).

663 The similar effect of microgravity on both visual and haptic object perception observed here could
664 hence be explained by a deformation of the body schema and/or internal representation of the
665 peripersonal 3D space due to the unusual lack of gravity. Indeed, IPS recurrent neural network
666 connections are set/learned for working in the presence of tonic, gravity-dependent, otolithic
667 inputs. If the network lacks this input, without appropriate adjustments to the synaptic weights,
668 the cross-modal transformations, and thus the concurrent object representations, would be
669 inexorably and similarly affected. In experiments studying visual perception in microgravity it
670 was indeed observed that distortions of object size perception are accompanied by a modification

671 of the subjective eye height estimation (Clement et al., 2008, 2013; Burrelly et al., 2015-2016),
672 that, in the light of our hypothesis, would reflect a distortion of the internal representation of the
673 body and/or peripersonal space.

674 **Conclusions**

675 Our study offers a better understanding of human perception of 3D geometry. We have provided
676 evidence for separate, modality-specific representations for visual and haptic object perception
677 in our tasks. Nevertheless, the observed link between the errors characterizing the two senses,
678 together with recent findings about reciprocal activations of the visual and haptic cortical
679 systems, indicate a tight interaction between concurrent visual and haptic object representations.
680 Furthermore, the observation that microgravity has the same incremental effect on visual and
681 haptic object perception argues for a modality-independent perceptive mechanism. Via this
682 mechanism, modality-specific object information would be treated by neural networks of the
683 parietal cortex and interpreted through an internal representation of the body and egocentric 3D
684 space, shaped by gravity (otolithic) signals. These microgravity experiments, therefore, provide
685 fundamental cues to better understand the neurophysiology of perception on Earth. They suggest
686 that fully independent, modality-specific 3D object perception does not exist, as the modalities
687 are inexorably linked by gravity. This implies that restricting future investigations to the brain
688 areas associated with a single sensory modality, even when studying only a modality-specific
689 behavior, would be a clear limiting factor in understanding the neural mechanisms underlying
690 3D object perception.

691 **References**

- 692 Amedi A, Jacobson G, Hendler T, Malach R, Zohary E (2002) Convergence of visual and tactile shape
693 processing in the human lateral occipital complex. *Cerebral cortex* 12:1202-1212.
- 694 Armstrong L, Marks LE (1999) Haptic perception of linear extent. *Perception & psychophysics* 61:1211–1226.
- 695 Arnoux L, Fromentin S, Farotto D, Beraneck M, McIntyre J, Tagliabue M (2017) The visual encoding of purely
696 proprioceptive intermanual tasks is due to the need of transforming joint signals, not to their
697 interhemispheric transfer. *Journal of neurophysiology* 118:1598--1608.
- 698 Avery GC, Day RH (1969) Basis of the horizontal-vertical illusion. *Journal of experimental psychology* 81:376–
699 380.
- 700 Barnett-Cowan M, Snow JC, Culham JC (2015) Contribution of Bodily and Gravitational Orientation Cues to
701 Face and Letter Recognition. *Multisensory research* 28:427–442.
- 702 Bernard-Espina J, Dal Canto D, Beraneck M, McIntyre J, Tagliabue M (2022) How Tilting the Head Interferes
703 with Eye-Hand Coordination: The Role of Gravity in Visuo-Proprioceptive, Cross-Modal Sensory
704 Transformations. *Frontiers in Integrative Neuroscience* 16:788905.
- 705 Blanke O, Perrig S, Thut G, Landis T, Seeck M (2000) Simple and complex vestibular responses induced by
706 electrical cortical stimulation of the parietal cortex in humans. *Journal of neurology, neurosurgery, and*
707 *psychiatry* 69:553-556.
- 708 Bourrelly A, McIntyre J, Luyat M (2015) Perception of affordances during long-term exposure to weightlessness
709 in the International Space station. *Cognitive processing* 16 Suppl 1:171–174.
- 710 Bourrelly A, McIntyre J, Morio C, Desprez P, Luyat M (2016) Perception of Affordance during Short-Term
711 Exposure to Weightlessness in Parabolic Flight. *PloS one* 11:e0153598.
- 712 Burns JK, Blohm G (2010) Multi-sensory weights depend on contextual noise in reference frame
713 transformations. *Front Hum Neurosci* 4:221.
- 714 Chen A, DeAngelis GC, Angelaki DE (2011) Representation of vestibular and visual cues to self-motion in
715 ventral intraparietal cortex. *The Journal of neuroscience* 31:12036-12052.
- 716 Chen X, Deangelis GC, Angelaki DE (2013) Diverse spatial reference frames of vestibular signals in parietal
717 cortex. *Neuron* 80:1310-1321.
- 718 Clarke AH, Griggull J, Mueller R, Scherer H (2000) The three-dimensional vestibulo-ocular reflex during
719 prolonged microgravity. *Exp Brain Res* 134(3):322-34
- 720 Clément G, Andre-Deshays C, Lathan CE (1989) Effects of gravitoinertial force variations on vertical gaze
721 direction during oculomotor reflexes and visual fixation. *Aviat Space Environ Med* 60(12):1194-8
- 722 Clément G, Vieville T, Lestienne F, Berthoz A (1986) Modifications of gain asymmetry and beating field of
723 vertical optokinetic nystagmus in microgravity. *Neuroscience letters* 63:271–274.
- 724 Clément G, Eckardt J (2005) Influence of the gravitational vertical on geometric visual illusions. *Acta Astronaut*
725 56(9-12):911–917.
- 726 Clément G, Lathan C, Lockerd A (2008) Perception of depth in microgravity during parabolic flight. *Acta*
727 *Astronautica* 63(7):828-832.

728 Clément G, Buckley A (2008) Mach's square-or-diamond phenomenon in microgravity during parabolic flight.
729 *Neurosci Lett* 447(2-3):179–182.

730 Clément G, Fraysse MJ, Deguine O (2009) Mental representation of space in vestibular patients with otolithic
731 or rotatory vertigo. *Neuroreport* 20:457–461.

732 Clément G, Reschke MF (2010) *Neuroscience in space*, Springer Science & Business Media.

733 Clément G, Skinner A, Richard G, Lathan C (2012) Geometric illusions in astronauts during long-duration
734 spaceflight. *Neuroreport* 23(15):894–899.

735 Clément G, Demel M (2012) Perceptual reversal of bi-stable figures in microgravity and hypergravity during
736 parabolic flight. *Neuroscience letters* 507:143–146.

737 Clément G, Skinner A, Lathan C (2013) Distance and Size Perception in Astronauts during Long-Duration
738 Spaceflight. *Life* 3(4):524–537.

739 Clément G, Loureiro N, Sousa D, Zandvliet A (2016) Perception of Egocentric Distance during Gravitational
740 Changes in Parabolic Flight. *PloS one* 11:e0159422.

741 Curry RE (1972) A Bayesian Model for Visual Space Perception. in 'Seventh Annual Conference on Manual
742 Control', pp187.

743 De Saedeleer C, Vidal M, Lipshits M, Bengoetxea A, Cebolla AM, Berthoz A, Cheron G, McIntyre J (2013)
744 Weightlessness alters up/down asymmetries in the perception of self-motion. *Experimental brain research*
745 226:95–106.

746 Deshpande G, Hu X, Stilla R, Sathian K (2008) Effective connectivity during haptic perception: a study using
747 Granger causality analysis of functional magnetic resonance imaging data, *NeuroImage* 40:1807-1814.

748 Dupin L, Hayward V, Wexler M (2018) Radial trunk-centred reference frame in haptic perception. *Scientific*
749 *reports* 8:13550.

750 Ernst MO, Banks MS (2002) Humans integrate visual and haptic information in a statistically optimal fashion.
751 *Nature* 415:429–433.

752 Fasse ED, Hogan N, Kay BA, Mussa-Ivaldi FA (2000) Haptic interaction with virtual objects. *Spatial perception*
753 *and motor control. Biological cybernetics* 82:69–83.

754 Girgus JS, Coren S (1975) Depth cues and constancy scaling in the horizontal-vertical illusion: the bisection
755 error. *Canadian journal of psychology* 29:59–65.

756 Goldreich DA (2007) Bayesian perceptual model replicates the cutaneous rabbit and other tactile
757 spatiotemporal illusions. *PLoS ONE* 2:e333

758 Goltz HC, Irving EL, Steinbach MJ, Eizenman M (1997) Vertical eye position control in darkness: orbital
759 position and body orientation interact to modulate drift velocity. *Vision research* 37:789–798.

760 Goodenough DR, Oltman PK, Sigman E, Cox PW (1981) The rod-and-frame illusion in erect and supine
761 observers. *Perception & psychophysics* 29:365–370.

762 Grefkes C, Weiss PH, Zilles K, Fink GR (2002) Crossmodal processing of object features in human anterior
763 intraparietal cortex: an fMRI study implies equivalencies between humans and monkeys. *Neuron* 35:173-
764 -184.

765 Grill-Spector K (2003) The neural basis of object perception. *Current opinion in neurobiology* 13:159-166.

766 Gurfinkel VS, Lestienne F, Levik Y, Popov KE (1993) Egocentric references and human spatial orientation in
767 microgravity. I. Perception of complex tactile stimuli. *Exp Brain Res* 95(2):339-42.

768 Harris LR, Jenkin M, Jenkin H, Dyde R, Zacher J, Allison RS (2010) The unassisted visual system on earth
769 and in space. *J Vestib Res* 20(1):25–30.

770 Harris LR, Mander C (2014) Perceived distance depends on the orientation of both the body and the visual
771 environment. *Journal of vision* 14.

772 Henriques DY, Klier EM, Smith MA, Lowy D, Crawford JD (1998) Gaze-centered remapping of remembered
773 visual space in an open-loop pointing task. *J Neurosci* 18(4):1583–1594.

774 Henriques DYP, Soechting JF (2003) Bias and sensitivity in the haptic perception of geometry. *Experimental*
775 *brain research* 150:95–108.

776 Howard I (1982) *Human visual orientation*. New York: Wiley.

777 Howard IP, Bergström SS, Ohmi M (1990) Shape from shading in different frames of reference. *Perception*
778 19:523–530.

779 James TW, Humphrey GK, Gati JS, Servos P, Menon RS, Goodale MA (2002) Haptic study of three-
780 dimensional objects activates extrastriate visual areas. *Neuropsychologia* 40:1706-1714.

781 Kersten D, Yuille A (2003) Bayesian models of object perception. *Current opinion in neurobiology* 13:150–158.

782 Kersten D, Mamassian P, Yuille A (2004) Object perception as Bayesian inference. *Annu Rev Psychol* 55:271-
783 304.

784 Kim JJJ, McManus ME, Harris LR (2022) Body Orientation Affects the Perceived Size of Objects. *Perception*
785 51:25-36.

786 Koch KW, Fuster JM (1989) Unit activity in monkey parietal cortex related to haptic perception and temporary
787 memory. *Experimental brain research* 76: 292-306.

788 Lacey S, Tal N, Amedi A, Sathian K (2009) A putative model of multisensory object representation. *Brain*
789 *topography* 21:269-274.

790 Lee TS (2015) The visual system's internal model of the world. *Proceedings of the IEEE. Institute of Electrical*
791 *and Electronics Engineers* 103:1359–1378.

792 Leone G (1998) The effect of gravity on human recognition of disoriented objects. *Brain research. Brain*
793 *research reviews* 28:203–214.

794 Lipshits MI, Gurfinkel EV, McIntyre J, Droulez J, Gurfinkel VS, Berthoz A (1994) Influence of weightlessness
795 on haptic perception. in 'Life Sciences Research in Space' pp367.

796 Lipshits M, McIntyre J (1999) Gravity affects the preferred vertical and horizontal in visual perception of
797 orientation. *Neuroreport* 10(5):1085–1089.

798 Liu Y, Sexton BM, Block HJ (2018) Spatial bias in estimating the position of visual and proprioceptive targets.
799 *Journal of neurophysiology* 119:1879–1888.

800 Loomis JM, Philbeck JW (1999) Is the anisotropy of perceived 3-D shape invariant across scale? *Perception*
801 *& psychophysics* 61:397–402.

802 Loomis JM, Klatzky RL, Giudice NA (2013) Representing 3D space in working memory: Spatial images from
803 vision, hearing, touch, and language 'Multisensory imagery'. Springer pp131–155.

804 Luyat M, Gentaz E (2002) Body tilt effect on the reproduction of orientations: studies on the visual oblique
805 effect and subjective orientations. *J Exp Psychol Hum Percept Perform* 28(4):1002-1011.

806 Marendaz C, Stivalet P, Barraclough L, Walkowiac P (1993) Effect of gravitational cues on visual search for
807 orientation. *Journal of experimental psychology. Human perception and performance.* 19:1266–1277.

808 Mast FW, Preuss N, Hartmann M, Grabherr L (2014) Spatial cognition, body representation and affective
809 processes: the role of vestibular information beyond ocular reflexes and control of posture. *Frontiers in*
810 *Integrative Neuroscience* 8:44.

811 McFarland J, Soechting JF (2007) Factors influencing the radial-tangential illusion in haptic perception.
812 *Experimental brain research* 178:216–227.

813 McGuire LMM, Sabes PN (2009) Sensory transformations and the use of multiple reference frames for reach
814 planning. *Nat Neurosci* 12(8):1056–1061.

815 McGuire LMM, Sabes PN (2011) Heterogeneous representations in the superior parietal lobule are common
816 across reaches to visual and proprioceptive targets. *J Neurosci* 31(18):6661--6673.

817 McIntyre J, Stratta F, Lacquaniti F (1997) Viewer-centered frame of reference for pointing to memorized targets
818 in three-dimensional space. *J Neurophysiol* 78(3):1601–1618.

819 McIntyre J, Lipshits M (2008) Central processes amplify and transform anisotropies of the visual system in a
820 test of visual-haptic coordination. *J Neurosci* 28(5):1246–1261.

821 Meyer K, Kaplan JT, Essex R, Damasio H, Damasio A (2011) Seeing touch is correlated with content-specific
822 activity in primary somatosensory cortex. *Cerebral cortex* 21:2113-2121.

823 Mierau A, Girgenrath M, Bock O (2008) Isometric force production during changed-Gz episodes of parabolic
824 flight. *Eur J Appl Physiol* 102:313-318.

825 Miyamoto T, Fukushima K, Takada T, de Waele C, Vidal PP (2007) Saccular stimulation of the human cortex:
826 a functional magnetic resonance imaging study. *Neuroscience letters* 423:68-72.

827 Moore C, Engel SA (2001) Neural response to perception of volume in the lateral occipital complex. *Neuron*
828 29:277-286.

829 Murdison TS, Leclercq G, Lefèvre P, Blohm G (2019) Misperception of motion in depth originates from an
830 incomplete transformation of retinal signals. *Journal of Vision* 19(12):1-15.

831 O'Reilly JX, Jbabdi S, Behrens TEJ (2012) How can a Bayesian approach inform neuroscience?
832 *Eur. J. Neurosci.* 35:1169-1179.

833 Paillard JJ, Paillard ed. (1991) *Brain and Space*, Oxford University Press, chapter Knowing where and knowing
834 how to get there pp461-481.

835 Prinzmetal W, Beck DM (2001) The tilt-constancy theory of visual illusions. *J Exp Psychol Hum Percept*
836 *Perform* 27(1):206–217.

837 Reschke MF, Kolev OI, Clément G (2017) Eye-Head Coordination in 31 Space Shuttle Astronauts during
838 Visual Target Acquisition. *Scientific reports* 7:14283.

839 Reschke MF, Wood SJ, Clément G (2018) Ocular Counter Rolling in Astronauts After Short- and Long-Duration
840 Spaceflight. *Scientific reports* 8:7747.

841 Sakata H, Takaoka Y, Kawarasaki A, Shibutani H (1973) Somatosensory properties of neurons in the superior
842 parietal cortex (area 5) of the rhesus monkey. *Brain research* 64:85-102.

843 Schlindwein P, Mueller M, Bauermann T, Brandt T, Stoeter P, Dieterich M (2008) Cortical representation of
844 saccular vestibular stimulation: VEMPs in fMRI. *NeuroImage* 39:19-31.

845 Smeets JBJ, van den Dobbelen JJ, de Grave DDJ, van Beers RJ, Brenner E (2006) Sensory integration
846 does not lead to sensory calibration. *Proc Natl Acad Sci USA* 103(49):18781–18786.

847 Snow JC, Strother L, Humphreys GW (2014) Haptic Shape Processing in Visual Cortex. *J. Cogn. Neurosci.*
848 26:1154-1167.

849 Stilla R, Sathian K (2008) Selective visuo-haptic processing of shape and texture. *Human Brain Mapping*
850 29:1123-1138

851 Sun HC, Welchman AE, Chang DHF, Di Luca M (2016) Look but don't touch: Visual cues to surface structure
852 drive somatosensory cortex. *NeuroImage* 128:353--361.

853 Tagliabue M, McIntyre J (2011) Necessity is the Mother of Invention: Reconstructing Missing Sensory
854 Information in Multiple, Concurrent Reference Frames for Eye-Hand Coordination. *J Neurosci* 31(4):1397–
855 1409.

856 Tagliabue M, McIntyre J (2012) Eye-hand coordination when the body moves: Dynamic egocentric and
857 exocentric sensory encoding. *Neurosci Lett* 513:78-83.

858 Tagliabue M, Arnoux L, McIntyre J (2013) Keep your head on straight: Facilitating sensori-motor
859 transformations for eye-hand coordination. *Neuroscience* 248:88-94.

860 Tagliabue M, McIntyre J (2013) When Kinesthesia Becomes Visual: A Theoretical Justification for Executing
861 Motor Tasks in Visual Space. *PLoS ONE* 8(7):e68438.

862 Tagliabue M, McIntyre J (2014) A modular theory of multisensory integration for motor control. *Front Comput*
863 *Neurosci* 8:1.

864 Taylor CM (2001) Visual and haptic perception of the horizontal-vertical illusion. *Perceptual and motor skills*
865 92:167-170.

866 Todd JT, Norman JF (2003) The visual perception of 3-D shape from multiple cues: are observers capable of
867 perceiving metric structure? *Perception & psychophysics* 65:31–47.

868 van Beers RJ, Sittig AC, Gon JJ (1999) Integration of proprioceptive and visual position-information: An
869 experimentally supported model. *J Neurophysiol* 81(3):1355–1364.

870 Vetter P, Goodbody SJ, Wolpert DM (1999) Evidence for an eye-centered spherical representation of the
871 visuomotor map. *Journal of neurophysiology* 81:935–939.

872 Villard E, Garcia-Moreno FT, Peter N, Clément G (2005) Geometric visual illusions in microgravity during
873 parabolic flight. *Neuroreport* 16(12):1395–1398.

874 Vingerhoets G (2008) Knowing about tools: neural correlates of tool familiarity and experience. *NeuroImage*
875 40:1380-1391.

876 Wagner M (1985) The metric of visual space. *Perception & psychophysics* 38(6):483–495.

877 Welchman AE (2016) The Human Brain in Depth: How We See in 3D. *Annual review of vision science* 2:345–
878 376.

879 Wolbers T, Klatzky RL, Loomis JM, Wutte MG, Giudice NA (2011) Modality-independent coding of spatial
880 layout in the human brain. *Current Biology* 21:984–989.

881 Wydoodt P, Gentaz E, Streri A (2006) Role of force cues in the haptic estimations of a virtual length.
882 *Experimental brain research* 171:481–489.

883 Yau JM, Kim SS, Thakur PH, Bensmaia SJ (2016) Feeling form: the neural basis of haptic shape perception.
884 *Journal of neurophysiology* 115:631-642.

885

JNeurosci Accepted Manuscript

Figure Legends

Figure 1: A) Haptic device and virtual reality headset used for the haptic and visual experiments, respectively. In panels B) and C) are reported the name of the orthogonal directions defined in an egocentric, body-centered (Longitudinal, LO; Lateral, LA; Anterior-Posterior, AP) and external, gravity-centered (Up-Down, UD; East-West, EW; North-South, NS) reference frames respectively. The bottom part of the figure represents the planes in which the task is performed expressed in the body-centered (Transversal, Sagittal and Frontal) and gravity-centered (Horizontal, Meridian and Latitudinal) reference frames.

Figure 2: Geometrical configurations of the task. The first row represents the six geometric configurations, which correspond to the combination of the three planes in which the rectangle could lie and the two different dimensions of the rectangle that the subject had to adjust. For each combination of geometric configuration and postural conditions (Upright and Supine), the table reports with black bold text the anatomical (egocentric) plane in which the task is performed as well as the anatomical direction of the adjustable (Adj.) and reference (Ref.) dimensions of the rectangles. The gray text in the lower part of the table corresponds to the definitions, in a gravity-centered reference frame arbitrarily looking north, of the task planes, as well as of the adjustable and reference dimensions of each rectangle. These allocentric definitions are independent of the postural condition. These terms are useful to refer to the various planes when testing the hypotheses of egocentric versus allocentric distortions.

Figure 3: Sign conventions for the errors in the Transverse, Frontal and Sagittal planes. The gray squares represent the correct answer (i.e. a square). The black lines represent the distorted answers. Positive planar error values correspond to “stubby” rectangles. Negative values correspond to “slender” rectangles. The same conventions are used for the error expressed in the allocentered planes. In this case, North-South (NS), East-West (EW) and Up-Down (UD) directions replace Anterior-Posterior (AP), Lateral (LA) and Longitudinal (LO), respectively. Horizontal, Latitudinal and Meridian replace Transversal, Frontal and Sagittal planes, respectively.

Figure 4: Method used for data filtering and for their vectorial representations. **A)** Fictitious individual errors recorded for the squaring task in the three anatomical planes (Sagittal, Transversal and Frontal) with the corresponding filtered value (see following panel). **B)** Each triplet of measured errors is represented as a point in a 3D space. The errors in the three anatomical planes should theoretically fulfill the constraint described by equation 3, corresponding to the solution plane represented in gray. The 3D point (black dot) is

hence projected on the solution plane (blue dot), removing the inconsistent components of the recorded errors. The three components of the projection (blue dot) are then used for the representation of the data in terms of the three planar error (filtered error in the first panel) and for the polar plot representation reported in the third panel. **C)** To improve readability, the data projected on the solution plane are reported as 2D polar plot, where the error triplets are represented as 2D vectors. In panels B-C the discontinuous lines represent the locations of triplets of errors lying in the solution plane and characterized by the following additional relationships: $\bar{\epsilon}_{Fro} = 0$ and hence $\bar{\epsilon}_{Sag} = -\bar{\epsilon}_{Tra}$ (dot-dashed line); $\bar{\epsilon}_{Tra} = 0$ and thus $\bar{\epsilon}_{Sag} = \bar{\epsilon}_{Fro}$ (dotted line); $\bar{\epsilon}_{Sag} = 0$ and $\bar{\epsilon}_{Tra} = \bar{\epsilon}_{Fro}$ (dashed line). The center of the polar plot corresponds to null errors in all three planes. **D)** Graphical representation of the 'Mis' parameter used to quantify the misalignment between two individual vectors and corresponding to the gray area of the parallelogram having the two vectors as sides.

Figure 5: **A)** Errors for the task performed in each of the six geometrical conditions using haptic information only (light blue bars) or visual information only (red bars). Each geometrical condition is characterized by the plane in which the rectangle lies (sagittal, transversal, frontal), and by which direction within the plane was adjustable or held constant: Longitudinal (Lo), Anterior-Posterior (AP), and Lateral (La). Positive errors correspond to the final size of the adjustable dimension being greater than the reference dimension. Vertical whiskers represent 95% confidence intervals. A significant difference between the two tasks performed in the same plane is indicative of an important perceptive distortion in that specific plane. **B)** Perceptive errors in the three task planes for haptic and visual conditions. *** : $p < 10^{-3}$ in the ANOVA testing the modality effect. † : $p < 10^{-3}$ for the t-test ascertaining differences from zero. **C)** Individual planar errors in the visual tasks as function of the errors in the haptic tasks. Each marker type corresponds to a specific subject. Their level of gray represents the plane of the task (black=sagittal, light-gray=frontal, dark-gray=transvers). The dashed line represents the data linear regression. The top-right insert represents the same data after subtracting to each point the mean error of the corresponding task plane. **D)** Vectorial representation of participant errors. Thicker vectors correspond to the vectorial average of the individual responses (thinner vectors). For details about the meaning of the polar plot representation see Figure 4C. **E)** Perceptive cuboids illustrating of how a cube (gray shape) would be perceived by the subjects when using haptic or visual information alone, respectively. For illustration purposes, the distortions of this panel are scaled up by a factor of 5. Data reported in all panels are based on the performances of 18 subjects.

Figure 6: Errors within each plane when the subjects are seated normally (Upright) or lying Supine. The upper **(A)** and lower **(B)** panels represent the results for the Haptic and Visual modalities, respectively. The left panels represent the errors per anatomical, egocentric plane. The right panels represent the data per

allocentric (fixed with respect to gravity) plane. ** : $p < 10^{-2}$ and *** : $p < 10^{-3}$ in the ANOVA. † and ‡ : $p < 10^{-2}$ and $p < 10^{-3}$ for the t-test ascertaining differences from zero. Vertical whiskers represent 95% confidence intervals. In each barplot the inset reports the perceptive cuboids corresponding to the 3D perceptive distortion (amplified x5) of a cube. The polar plots report the vectorial representation of the individual errors. Thicker vectors represent the average vectorial response. For details about the meaning of the polar plot representation see Figure 4C. Data reported in this figure are based on the performances of 36 subjects (18 for haptic and 18 for visual experiment).

Figure 7: Results of the microgravity experiments for the haptic (A-C and F panels) and visual (D-E and G panels) tasks. **A)** Contact forces in the three experimental conditions: normogravity (1G), microgravity (0G) and with a mechanical support of the arm (Supp). Left: Vertical forces generated against the upper and lower edges of the rectangle. Right: Horizontal forces generated against all other edges of the rectangle. **B) and D)** Errors observed in the three task planes for each experimental condition, together with the error predicted in microgravity assuming the same effect of gravity on both haptic and visual tasks. **C) and E)** are polar plots representing individual errors. Thicker vectors represent the average vectorial response. For details about the meaning of the polar plot representation see Figure 4C. **F-G)** Illustration of the perceptive cuboids (experimental results scaled up by 5) in normal gravity and in microgravity together with the reference cube (gray). * : $p < 0.05$, ** : $p < 10^{-2}$ and *** : $p < 10^{-3}$ in the ANOVA. †, ‡ and ‡ : $p < 0.05$, $p < 10^{-2}$ and $p < 10^{-3}$ for the t-test ascertaining difference from zero. Data reported are based on the performances of 36 subjects: 18 for the haptic and 18 for the visual experiment.

Figure 8: Comparison of the effect of microgravity on the Haptic and Visual senses. **A)** Difference between the constant errors made by the subjects in the 0G and 1G conditions for the tasks in the three anatomical planes. Vertical whiskers represent 95% confidence interval. **B)** Vectorial representation of the gravity effect. Thicker vectors represent the average response. For details about the meaning of the polar plot representation see Figure 4C. Data reported are based on the performances of 36 subjects (18 for the visual and 18 for the haptic experiment).

Figure 9: **A)** Evidences of neural activation associated to haptic (blue), visual (red) and cross-modal (orange) objects' perception. The regions primarily involved in haptic objects representation are the primary and secondary somatosensory areas (S1 and S2), the Brodmann area 5 (BA5), and the ventral premotor (vPM) area. The 3D object visual representation is known to reside in the lateral occipital complex (LOC). Numbers' font size qualitatively represents the intensity of the neural activation during object perception tasks: 1

Sakata et al. 1973; 2 Koch & Fuster 1989; 3 Moore & Engel 2001; 4 James et al. 2002; 5 Grefkes et al. 2002; 6 Amedi et al. 2002; 7 Grill-Spector 2003; 8 Deshpande et al. 2008; 9 Stilla & Sathian 2008; 10 Vingerhoets 2008; 11 Lacey et al. 2009; 12 Meyer et al. 2011; 13 Snow et al. 2014; 14 Sun et al. 2016; 15 Yau et al. 2016. Green letters represent studies reporting otolithic projection in the intraparietal sulcus (IPS) area: a Blanke et al. 2000; b Miyamoto et al. 2007; c Schlindwein et al. 2008; d-e Chen et al. 2011, 2013. **B)** Proposed schematic of information processing underlying objects perception. Space/body internal representations reciprocally connect concurrent haptic and visual object representation and allow building a visual representation of the object from haptic signals and vice versa. Otolithic signals affect the body/space internal representation, distorting both haptic and visual object representations. Beneath the blocs are reported their identified cortical location based on electrophysiological and brain imaging findings reported in the literature.

Table Legends

Table 1: Definition of the squaring errors for all six geometrical configurations of the task.

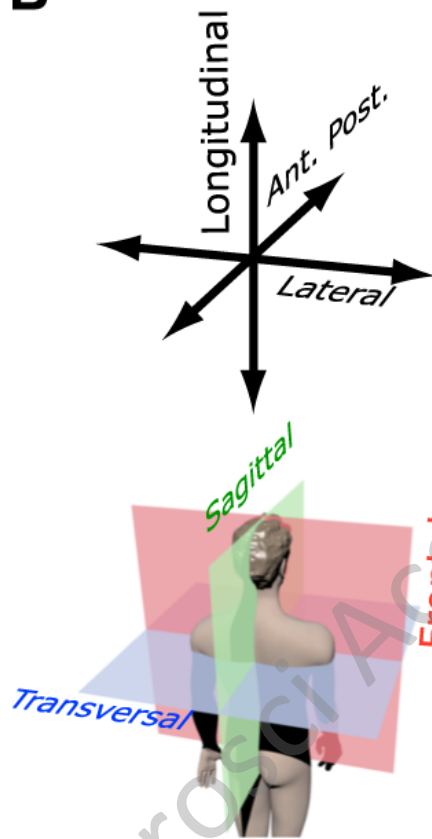
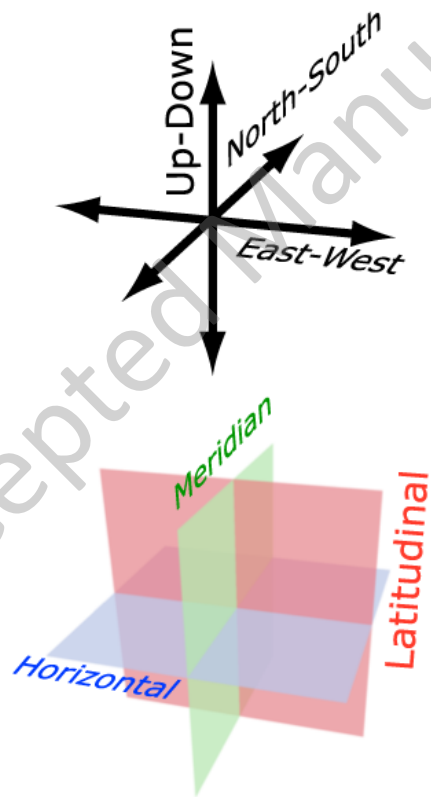
Plane	Adjustable dimension	Reference dimension	Task error
Frontal	LA	LO	$\varepsilon_{LA-LO} = \varepsilon_{LA} - \varepsilon_{LO}$
	LO	LA	$\varepsilon_{LO-LA} = \varepsilon_{LO} - \varepsilon_{LA}$
Transversal	LA	AP	$\varepsilon_{LA-AP} = \varepsilon_{LA} - \varepsilon_{AP}$
	AP	LA	$\varepsilon_{AP-LA} = \varepsilon_{AP} - \varepsilon_{LA}$
Sagittal	LO	AP	$\varepsilon_{LO-AP} = \varepsilon_{LO} - \varepsilon_{AP}$
	AP	LO	$\varepsilon_{AP-LO} = \varepsilon_{AP} - \varepsilon_{LO}$

Table 2: Relationship between ego- and allo- centrically defined distortions for the Upright and Supine condition.

Upright	$\bar{\varepsilon}_{Mer} = \bar{\varepsilon}_{Sag}$	$\bar{\varepsilon}_{Lat} = \bar{\varepsilon}_{Fro}$	$\bar{\varepsilon}_{Hor} = \bar{\varepsilon}_{Tra}$
Supine	$\bar{\varepsilon}_{Mer} = -\bar{\varepsilon}_{Sag}$	$\bar{\varepsilon}_{Lat} = \bar{\varepsilon}_{Tra}$	$\bar{\varepsilon}_{Hor} = \bar{\varepsilon}_{Fro}$

Table 3: Results of ANOVA for the posture effect on the planar perceptive distortion.

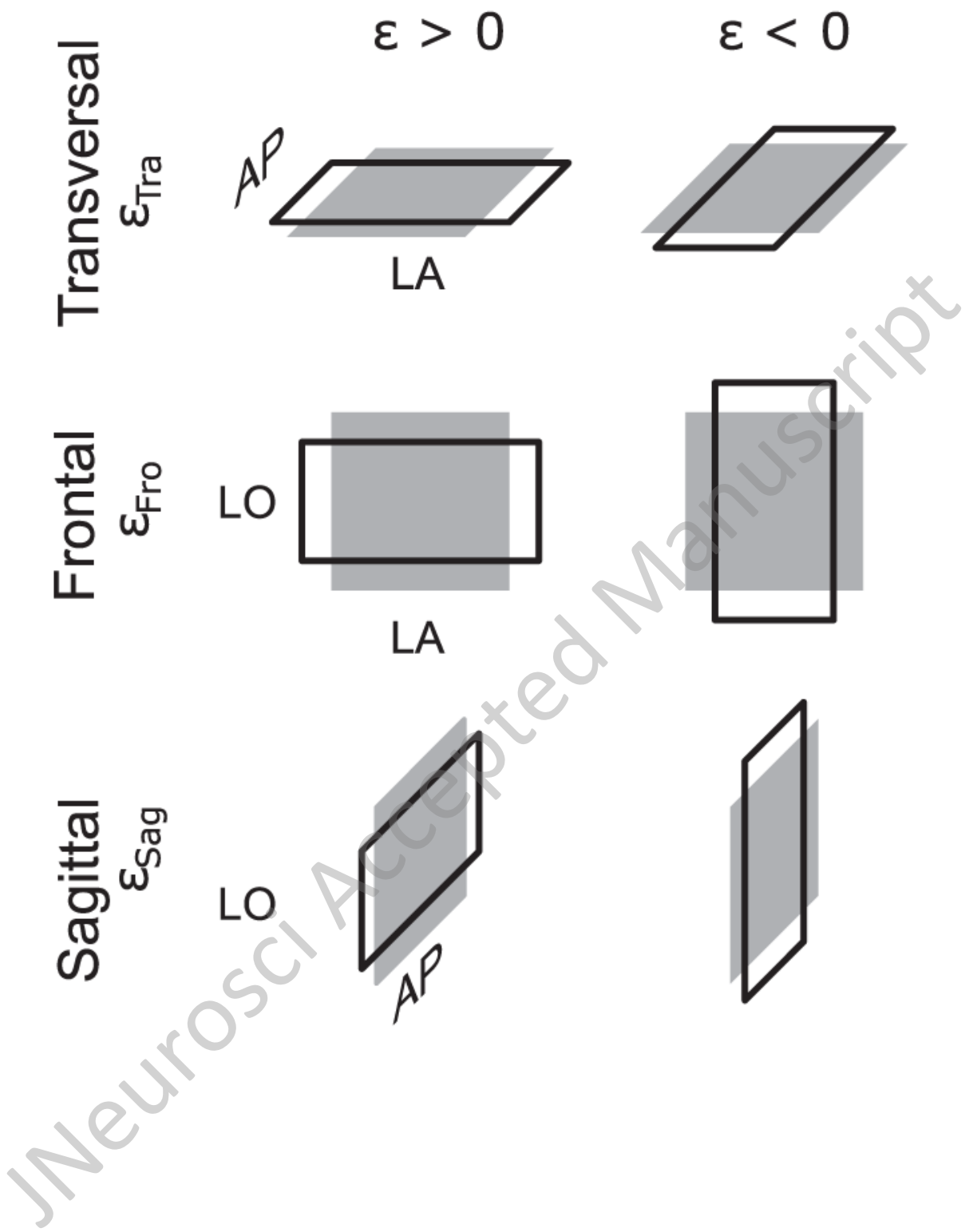
	Sagittal	Transversal	Frontal	Meridian	Horizontal	Latitudinal
Haptic	F(1,17)=0.40 p=0.53	F(1,17)=0.58 p=0.46	F(1,17)=0.001 p=0.97	F(1,17)=52.28 p<10-5	F(1,17)=13.01 p=0.002	F(1,17)=12.18 p=0.003
Visual	F(1,17)=2.00 p=0.18	F(1,17)=1.32 p=0.27	F(1,17)=0.15 p=0.70	F(1,17)=25.46 p<10-3	F(1,17)=19.92 p<10-3	F(1,17)=22.87 p<10-3

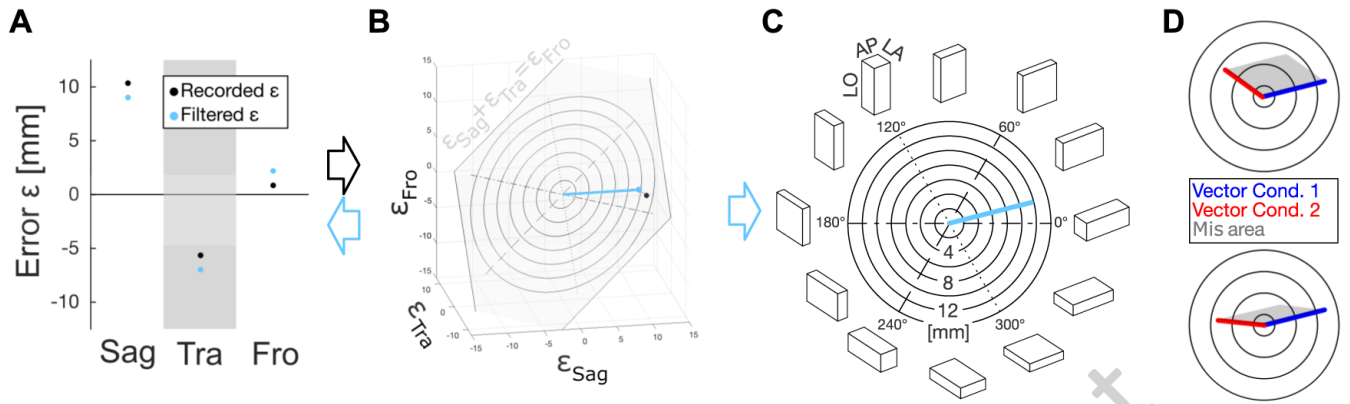
A**B****C**

Accepted Manuscript

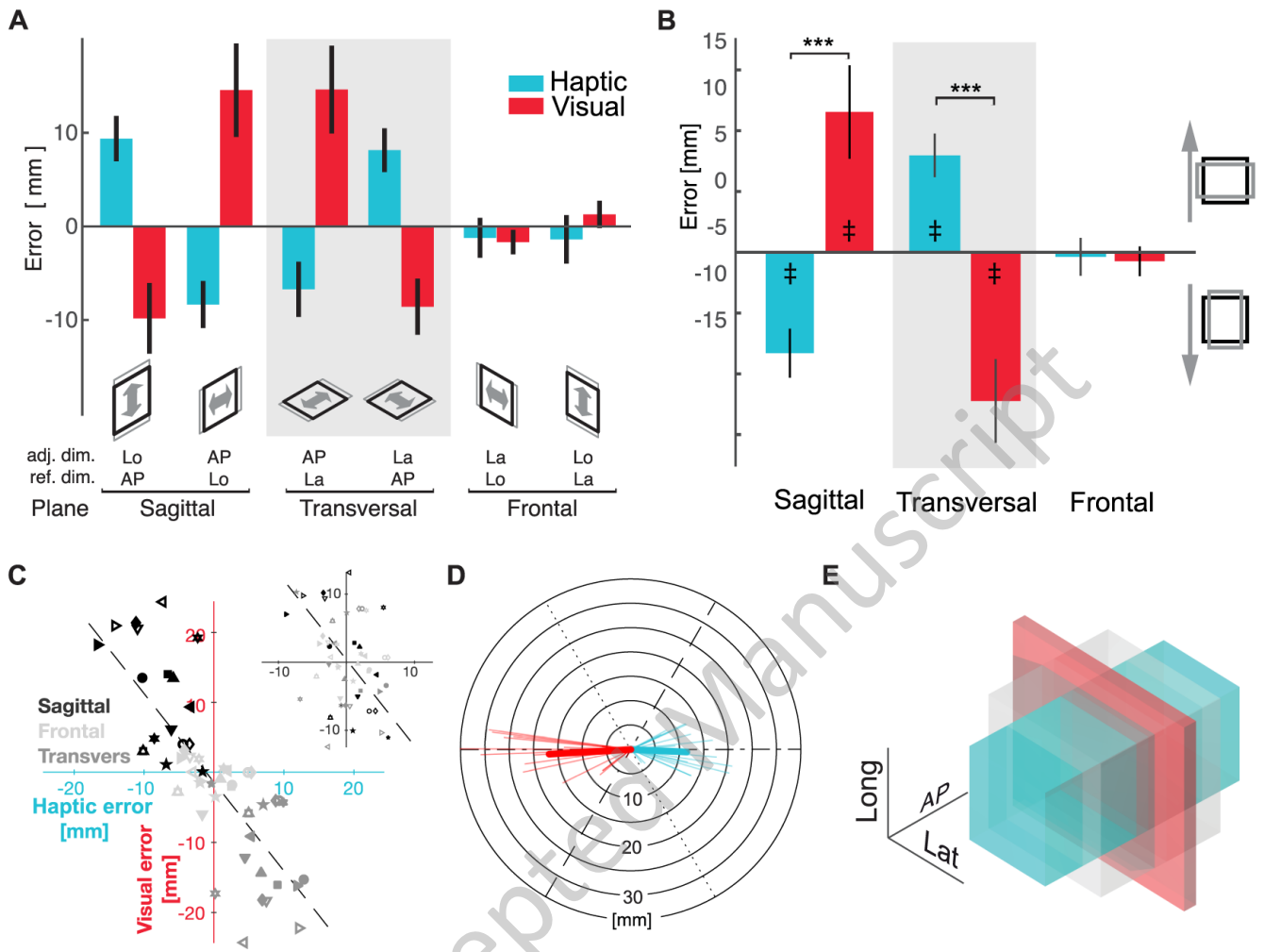
							
Upright		Plane Frontal		Plane Transversal		Plane Sagittal	
	Ref. Dim.	Lateral	Longitudinal	Lateral	Ant-Post	Longitudinal	Ant-Post
	Adj. Dim.	Longitudinal	Lateral	Ant-Post	Lateral	Ant-Post	Longitudinal
Supine		Plane Transversal		Plane Frontal		Plane Sagittal	
	Ref. Dim.	Lateral	Ant-Post	Lateral	Longitudinal	Ant-Post	Longitudinal
	Adj. Dim.	Ant-Post	Lateral	Longitudinal	Lateral	Longitudinal	Ant-Post
	Plane	Plane Latitudinal		Plane Horizontal		Plane Meridian	
	Ref. Dim.	East-West	Up-Down	East-West	North-South	Up-Down	North-South
	Adj. Dim.	Up-Down	East-West	North-South	East-West	North-South	Up-Down

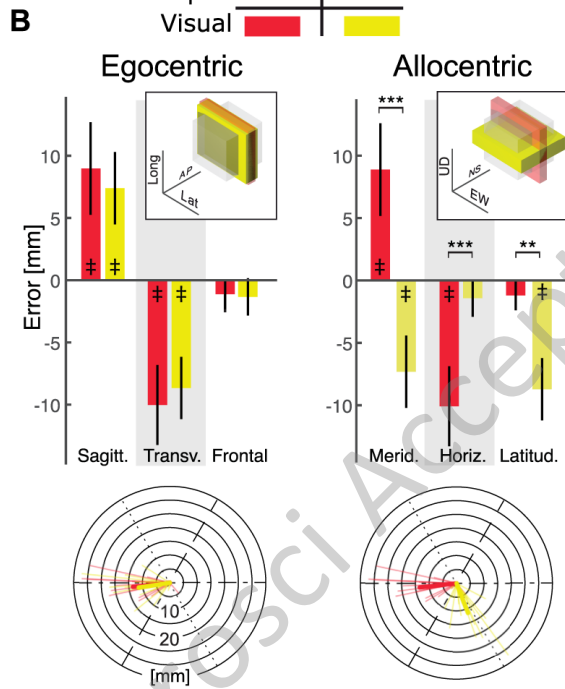
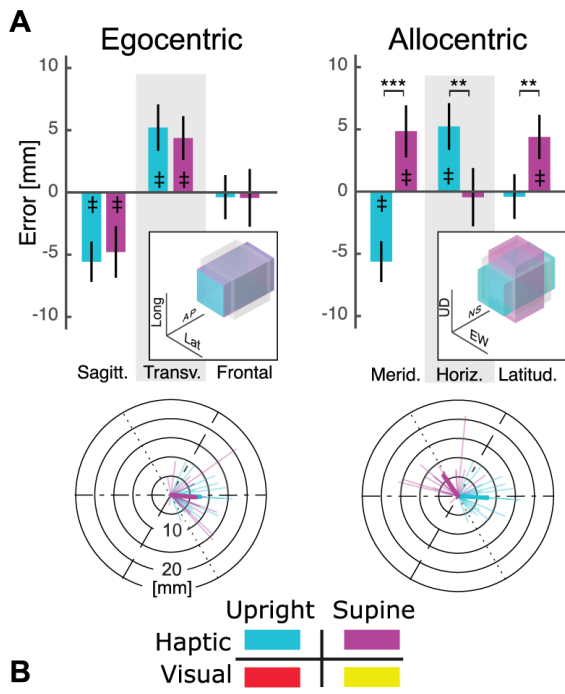
JNeurosci Accepted Manuscript



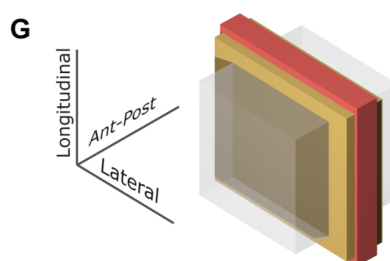
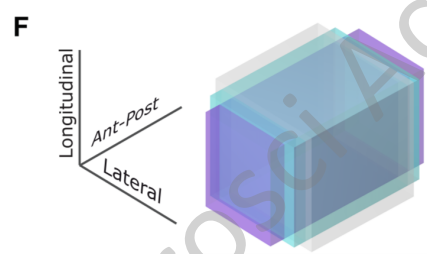
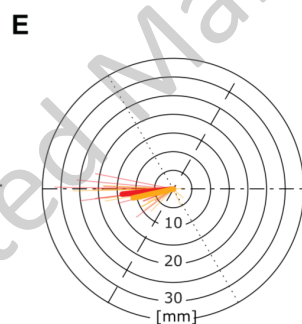
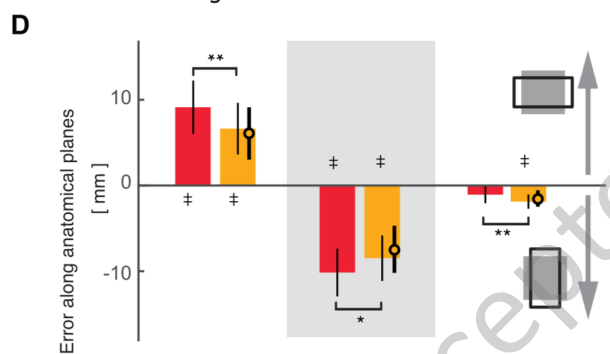
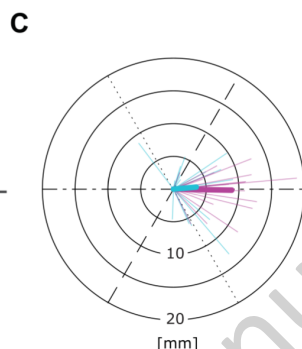
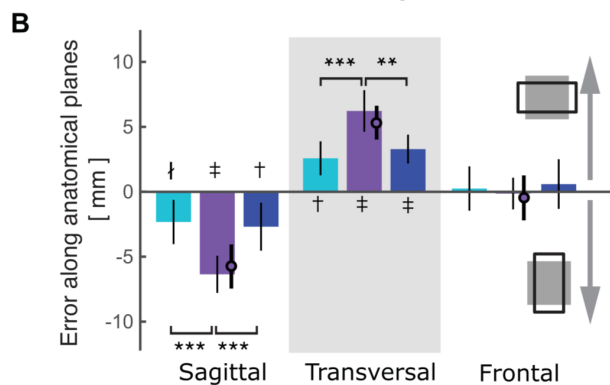
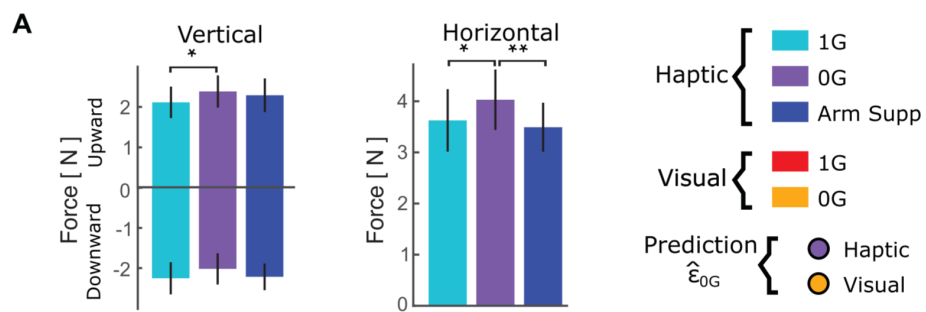


JNeurosci Accepted Manuscript

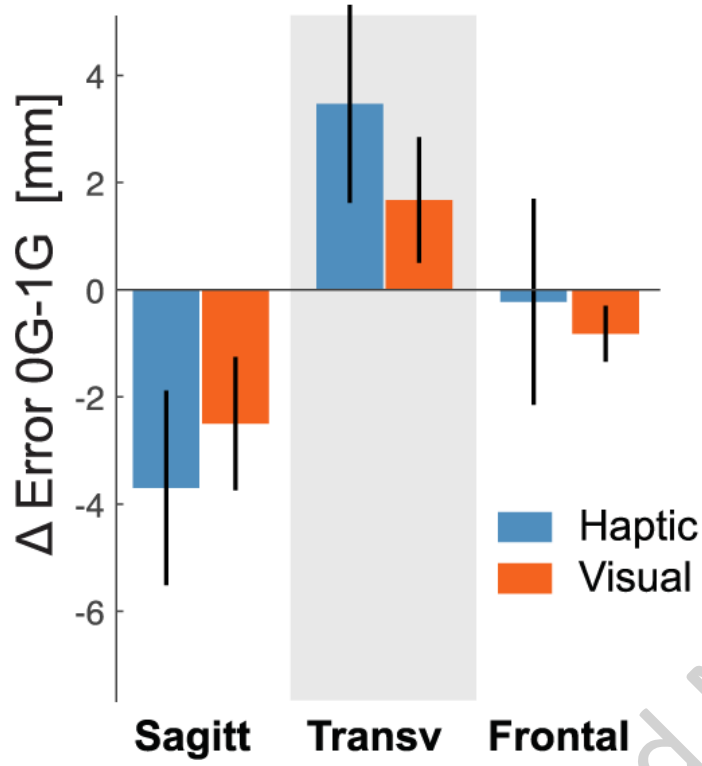
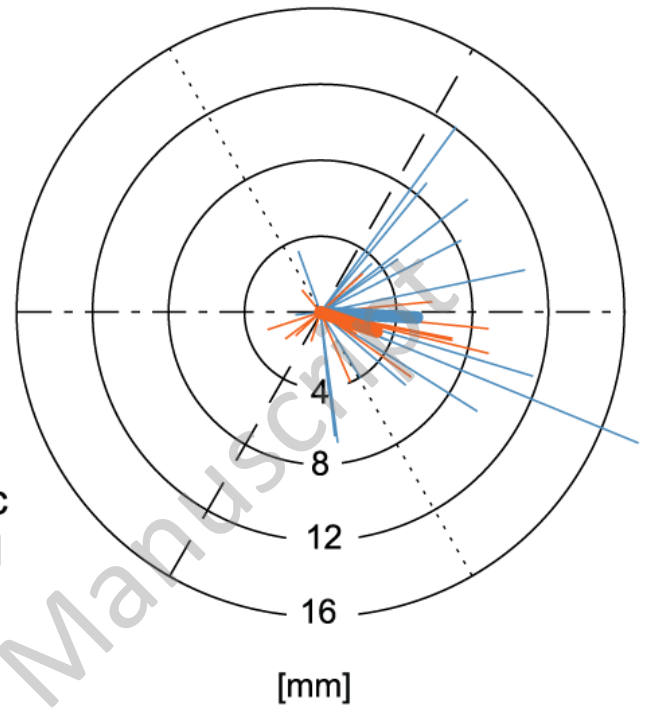




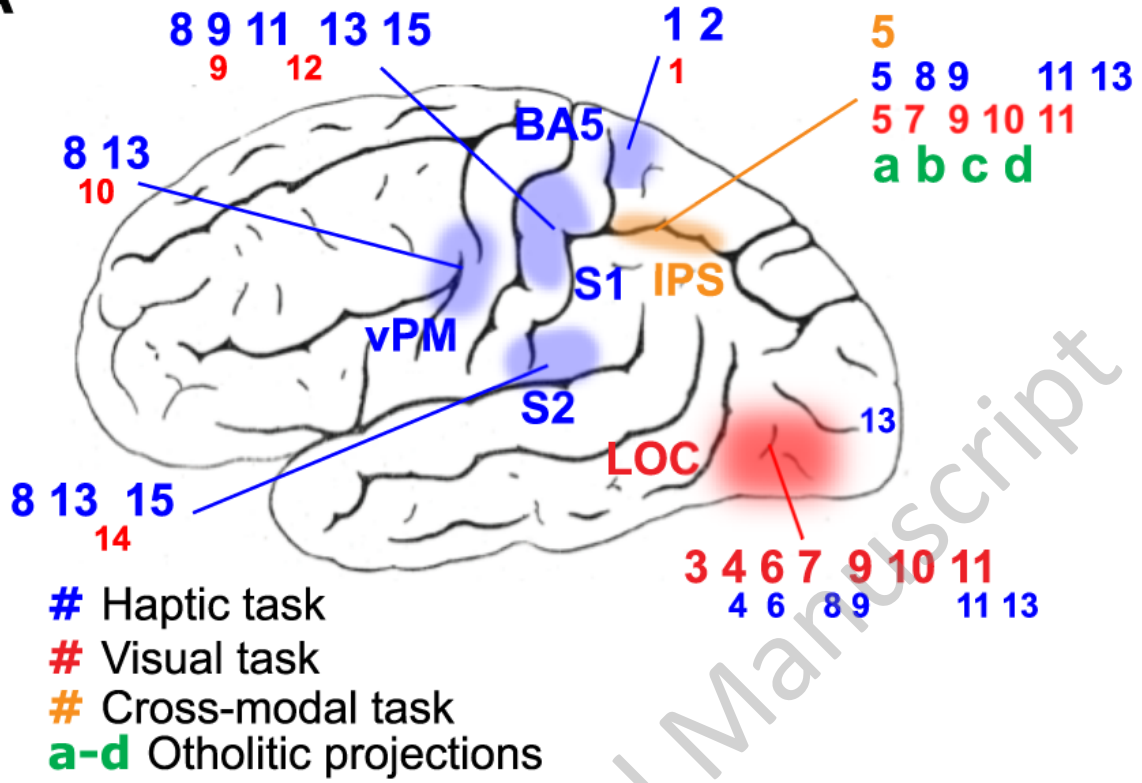
JNeurosci Accepted Manuscript



JNeurosci Accepted Manuscript

A**B**

JNeurosci Accepted Manuscript

A**B**